Characterization of the Electromagnetic Fields Inside a Wire Mesh Cage for Biotelemetry

Johnny Bernard Lienau
Marquette University

CHARACTERIZATION OF THE ELECTROMAGNETIC FIELDS INSIDE A WIRE MESH CAGE FOR BIOTELEMETRY

By

Johnny Lienau, B.S.

A Thesis Submitted to the Faculty of the Graduate School of
Marquette University,
in Partial Fulfillment of the Requirements for
the Degree of Master of Science.

Milwaukee, Wisconsin

December 2009

ABSTRACT
CHARACTERIZATION OF THE ELECTROMAGNETIC FIELDS
INSIDE A WIRE MESH CAGE FOR BIOTELEMETRY

Johnny Lienau, B.S.

Marquette University, 2009

A wire mesh cage composed of thin conductive wires will influence the behavior of electromagnetic fields within it. Theory suggests that the cage will behave like a low Q cavity. Many researchers have investigated electromagnetic field behavior in solid walled cavities and waveguides, but little of this work has probed into the effects of a wire mesh. Additionally, few studies have investigated RF communication in these types of environments. The primary goal of this work is to research wireless communication inside a low Q wire mesh cavity in the 200-700 MHz range. Through simulated and experimental results, ideal antenna locations and behavior are described for simple antennas.

The Numerical Electromagnetics Code (NEC) is used to examine the electromagnetic field behavior inside a wire mesh rat cage. The code provides a foundation of theoretical results from which to base experimentation on. It is shown through simulations that dipole, loop, and monopole antennas are heavily affected by the cage. When placed inside, the antenna input impedance and current distribution are dramatically altered near cage resonance. Position of the antenna affects coupling to the mode and the changes in input impedance and current distribution.

Experimentally, monopole and loop antennas are evaluated inside the wire mesh animal cage. The monopole couples to the cage very well due to the impedance changing effects caused by the low Q cavity. The loop is shown to be resistant to same effects, and does not couple well. Due to the configuration of the first resonant mode, it is shown that coupling to the cage is best accomplished with an electric field dominant antenna.

RF communication is best accomplished with a receive monopole antenna located at the top center of the cage. The transmit antenna can move to any position without a significant loss of received power. This is a direct result of coupling to the first resonant mode. To construct a wireless communication system, the designer should consider coupling to the resonant modes and using a low Q cavity.

ACKNOWLEDGEMENTS

Johnny Lienau, B.S.

I would like to thank my mother and father (Mary and Jim Lienau) for their unending support, love, and guidance. My brother (James Lienau) for his support and continual enthusiasm for my success. I would also like to thank Dr. Richie and Dr. Jeutter for taking me on as their student and guiding me through my graduate career. I never could have imagined all that I was going to learn two years ago when I first began looking for a project. I want to thank Dr. Luglio for being on my committee and attending every seminar I presented. I also want to thank all the Microwave Seminar attendees who consistently provided meaningful feedback and insight on my research. Some of the most important experiences I had were standing in front of my peers presenting my work. I would also like to thank Dr. Schneider for her guidance as my undergraduate advisor and her encouragement of graduate studies.

TABLE OF CONTENTS

LIST OF TABLES

LIST OF FIGURES

1 Introduction

1.1 Motivation

Small animals such as rats and mice are often used for experiments in the advancement of healthcare technology. New vaccines and drugs are first tested in non-human subjects to observe possible effects that might occur in people. The process of monitoring small animals inside a cage can be tedious and time consuming. Individually checking the blood pressure, pulse, etc. of each animal is not efficient. An implantable transmitter device capable of automatically recording this and other data would be very advantageous. Wireless communication with this implant would dramatically reduce the time spent collecting data and information could be gathered in real time. A whole wall of animal cages could have its data retrieved and analyzed almost instantaneously.

In order for a monitoring system to work effectively, communication between the implanted device and a data processor must be achieved. This is difficult because a metal animal cage will interfere with radio frequency (RF) communications. Transmit and receive antennas placed inside the cage do not act like their free space counterparts. There are also a large number of electromagnetic effects that can occur inside metallic enclosures. Lastly, the animal must be able to move around freely within the cage, uninhibited by the communication system.

The transmit and receive antennas will both be inside the animal cage. The implanted device (acting as the transmit antenna) will send biological information to a receive antenna, which will be connected to an external coaxial cable outside the cage. A comprehensive study

on communication inside a wire mesh cage must be performed in order to predict the antenna and electromagnetic field behavior. Metal enclosures such as waveguides and cavities have been thoroughly studied in an attempt to understand how electromagnetic fields behave inside them [1,2]. However, some of the most difficult problems still arise in communications when transmitters, receivers, and other sensitive equipment are placed in a metal enclosure that reduces their ability to operate effectively.

1.2 Previous Work

Solid enclosures have been studied extensively since the 1970s. Most of the work focused on the penetration of EM fields through apertures in the walls of the enclosure. Reference [3] is an early piece of work that investigated insertion loss of a rectangular enclosure with apertures containing an internal radiating source. Similarly, [4] examined external sources and their penetration into a cavity. Both pieces of work produced estimates for shielding effectiveness below cutoff of the 1^{st} resonant mode.

More recently, extensive work has been done by Robinson et al [5, 6] and Sewell et al [1]. Building on some of his own previous work and mathematics from [3], Robinson developed a numerical solution to model a cavity with an aperture and its resulting shielding effect anywhere within the enclosure. Using transmission line theory, Robinson and his colleagues' formulation considers only the TE_{10} mode, but is valid above and below the first cutoff frequency. Robinson's numerical model also allows for internal losses, the consideration of multiple apertures, and is a function of the cavity and aperture dimensions.

Today, there exists a variety of methods to determine the electromagnetic fields while considering multiple modes within an enclosure containing apertures. The Method of Moments (MoM), the finite difference time domain (FDTD), and transmission line matrix (TLM) are all

techniques that have proven reliable [1, 6]. While each method is capable, there are often differences in the solutions depending on the resolution chosen for the computer simulations and due to the methods themselves. These methods were designed for predicting field strength inside simple metallic structures with a limited number of apertures, and more importantly from an external source. The authors who accomplished most of this work, never considered a low Q cavity or wire mesh cage.

Casey [7] provides an investigation into the shielding behavior of wire-mesh screens. In his work, Casey concluded that the plane-wave shielding effectiveness of a mesh screen tended to decrease with an increasing frequency. This is opposite of a solid metal sheet, whose shielding effectiveness increases as frequency does. When a mesh was used to form an enclosure, the shielding effectiveness increased with frequency, saturated at a maximum value, and then began to decrease. Casey also developed equations to estimate the sheet impedance of a wire mesh screen, which will be used later on in Chapter 2. While Casey's work provides insight into wire mesh, he only considered a plane wave in the far field. RF communication within a small wire mesh cage will primarily be dominated by the near field and antenna characteristics.

Using numerical and experimental techniques, several authors [8-11] have investigated antenna behavior within a cavity. In [8], coupling between two antennas within a cavity is investigated. Through numerical evaluation, [8] comes to the conclusion that in a cavity coupling between two antennas is not necessarily dependent on the distance between them. The modal configuration dominates coupling within an enclosure. References [9] and [10] both discuss input impedance of simple antennas inside a cavity as the frequency approaches resonances. In the results, the antenna input impedance was shown to increase drastically at resonance. Reference [9] attributed the increase to "coupling resistance" between the antenna

and cavity, which was extremely high at resonance. In addition to the impedance increase at resonance, [10] investigated current distribution on the antenna. The cavity was shown to be forcing a full wave current distribution on the dipole antenna at resonance, even though it was only a quarter wavelength long. While these works provide some meaningful insight pertaining to communication inside a wire mesh cage, several important details are lacking. None of them moved the antennas; they were only placed at the point of maximum coupling to the mode. Additionally, only solid enclosures were considered.

1.3 Problem Statement

Little work has been done in the area of examining the field configuration within a metallic enclosure from an internal source. Much of the previous research is lacking in key areas that must be considered to implement RF communications inside a cage. No work has been found for the characterization of the electromagnetic fields within a wire-mesh enclosure. This thesis will investigate the possibility of radio frequency (RF) communication by examining the field configuration within a wire-mesh animal cage from an internal radiator.

Simple antennas, such as dipole, monopole, and loop, will be considered as sources exciting the fields within a wire mesh cage. The development of modes, nulls, the quality factor, current distribution and input impedance will be investigated. The results of this thesis will provide a foundation in which a wireless communication system can be developed for small animals within a wire-mesh cage.

Chapter 2 will introduce and discuss the electromagnetic theory behind TE modes within a low Q cavity. This is followed by a discussion of the Numerical Electromagnetic Code (NEC) and its use in this thesis. Chapter 3 describes the making of monopole and loop antennas and explains the experimental setup. Chapter 4 presents the NEC simulation results for a dipole

placed within the animal cage. Conclusions from chapter 4 will be used as a foundation for the experimental monopole and loop antenna results. Chapter 5 presents the simulation and experimental results of the monopole antenna. Chapter 6 discusses the simulated and experimental results of the loop antenna. Chapter 7 will sum the conclusions from all three previous chapters and present ideas for future work. Chapter 8 is the bibliography.

2 Theory and Methodology

2.1 Description and Properties of Wire Mesh Cage

2.1.1 Cage Description

The structure used for this thesis is 38cm x 29cm x 21cm wire mesh animal cage. The cage was designed and provided by NASA Ames Sensors 2K! group and Dr. Dean Jeutter for the Advanced Animal Habitat project. The mesh is composed of interlacing wires 1mm in diameter, welded together at intersections to form 1.2cm x 1.2cm squares. The front of the cage has two vertical apertures, dimensions 4cm x 21cm, one located at the far left and the other at the right. The front also has two doors that can swing open; each one is hinged next to their corresponding aperture and latches shut at the center. The wires are composed of stainless steel. The exact type of stainless steel is not known, but type 304 is assumed because it is the most common. The composition and properties of type 304 are listed in Table 2-1; other types of stainless steel differ by percentage of the materials listed. There are also two thin solid plates on the back side of the cage. These plates serve as mounting points for watering tubes for animals inside. The apertures in the front are access points to add or remove feeding trays. Diagrams of the cage are shown in Chapter 2 Section 2.4, NEC-Animal Cage Model.

%Cr	18-20
%Ni	10.5
%C	0.08
%Mn	2
%Si	0.75
%P	0.045
%S	0.03
Conductivity	$1.450*10^{6}$ S/m
Permeability	2000 H/m

Table 2-1: Stainless Steel Type 304 Properties

2.1.2 Waveguide Modes

A mode is a specific configuration of electromagnetic fields within a structure. Modes are most often formed in waveguides or cavities. There are three types of modes, transverse electric (TE), transverse magnetic (TM), and transverse electromagnetic (TEM). TE^z modes are field configurations whose electric field components are transverse to the z-direction. The same configuration is seen for TM^z modes except the magnetic components are transverse to z. TEM^z waves have electric and magnetic components transverse to the z-direction. In general, waveguides support both TE^z and TM^z modes where z is also the direction of propagation. TEM^z modes can be seen in transmission line theory, which can support all three.

A diagram of a waveguide is shown below in Figure 2.1:

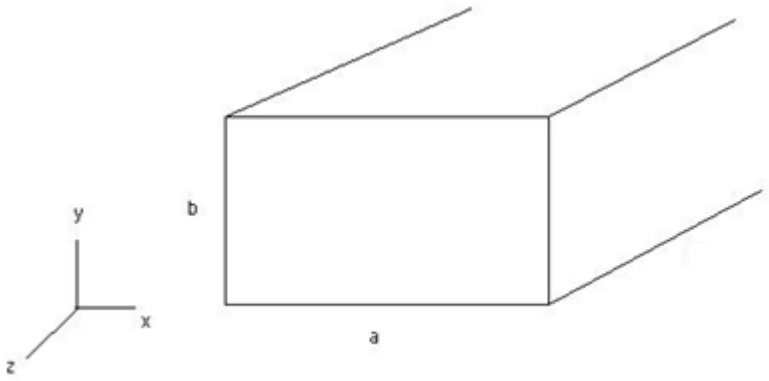

Figure 2.1 Waveguide Diagram, a > b

The transverse components are in the x-y plane with the wave propagating in the z-direction. The waveguide is along the z axis, the y and x axes are bounded by b and a respectively. Nomenclature for writing a mode indicates the type of mode (TM^z or TE^z), and a subscript with the mode number.

Expressions for transverse electromagnetic modes in a waveguide can be derived from the Helmholtz wave equation.

$$\nabla^2 F_Z + \beta^2 F_Z = 0 \tag{1}$$

Where β is the wave number in equation (4). F_Z represents the z component of the vector electric potential $\vec{F}$ [C/m]. The solution to (1) can be obtained through use of the separation of variables technique. F_Z is a function of x, y, and z: and can be written out as such.

$$F_Z(x, y, z) = f(x)g(y)h(z) \tag{2}$$

With the knowledge that the tangential component of the $\vec{E}$-field must go to zero at the walls, this allows for the writing of boundary conditions, which in turn allow solutions to be chosen for (2). The resulting boundary conditions are as follows:

Condition 1 (Top and Bottom Walls):
$E_x(x, y=0, z) = E_x(x, y = b, z) = 0$
$E_z(x, y=0, z) = E_z(x, y = b, z) = 0$
Condition 2 (Left and Right Walls):
$E_y(x = 0, y, z) = E_y(x = a, y, z) = 0$
$E_z(x = 0, y, z) = E_z(x = a, y, z) = 0$

Table 2-2: Waveguide Boundary Conditions

Since the electric field is bounded in the x and y directions, $f(x)$ and $g(y)$ are chosen to represent standing waves. $h(z)$ is given the form of a traveling wave in the +z direction.

$$F_Z(x, y, z) = [C_1 \cos(\beta_x x) + D_1 \sin(\beta_x x)]\big[C_2 \cos(\beta_y y) + D_2 \sin(\beta_y y)\big] A e^{-j\beta z} \tag{3}$$

where the separation equation is

$$\beta_x^2 + \beta_y^2 + \beta_z^2 = \beta^2 = \omega^2\mu\varepsilon \tag{4}$$

Equation (3) can be used to compute the electric and magnetic field components by application of Maxwell's curl equations.

$$\vec{E} = \frac{1}{\varepsilon}\nabla \times \vec{\mathrm{F}} \tag{5}$$

$$\vec{H} = \frac{1}{j\omega\mu}\nabla \times \vec{E} \tag{6}$$

Application of (5) to find E_x gives the following expression:

$$E_x = -A\frac{\beta_y}{\varepsilon}[C_1\cos(\beta_x x) + D_1\sin(\beta_x x)]\left[-C_2\sin(\beta_y y) + D_2\cos\left(\beta_y y\right)\right]e^{-j\beta z} \tag{7}$$

Using Condition 1 from Table 2-2 causes E_x to go to zero at the wall, which forces D_2 to be set to 0. This then creates a limited set of values that will provide nontrivial solutions. The term $\sin\left(\beta_y b\right)$ must equal 0, and this can only be accomplished if

$$\beta_y = \frac{n\pi}{b} \quad n = 0,1,2\ldots \tag{8}$$

In the same manner by use of Condition 2 from Table 2-2, $\vec{E}_y$ will only be zero if

$$\beta_x = \frac{m\pi}{a} \quad m = 0,1,2\ldots \tag{9}$$

Thus, β_x and β_y are functions of the waveguide dimensions and proportional to the frequency and intrinsic properties of the medium. In conjunction with the boundary conditions, (3) can be simplified to

$$F_Z(x,y,z) = A_{mn}\cos(\beta_x x)\cos\left(\beta_y y\right)e^{-j\beta z} \tag{10}$$

The subscripts mn represent the eigenvalues for β_x and β_y and in turn the field configuration (mode). A specific combination of m and n designates a unique TE_{mn}^z mode. β_x and β_y are related to the wave number β_z and that of free space by the separation equation (4). Setting β_z to zero and substituting (8) and (9) into (4) will yield a cutoff frequency for a given mode.

$$f_{mn} = \frac{1}{2\pi\sqrt{\mu\varepsilon}}\sqrt{\left(\frac{m\pi}{a}\right)^2 + \left(\frac{n\pi}{b}\right)^2} \tag{11}$$

$$\left.\begin{matrix} m = 0, 1, 2, \ldots \\ n = 0, 1, 2, \ldots \end{matrix}\right\} \; m = n \neq 0$$

For a given f_{mn}, the mode will not propagate below that frequency. The lowest mode that will propagate in a waveguide is the dominant mode. If β_z is imaginary, the fields within the waveguide are evanescent and not propagating. If β_z is greater than zero propagating waves exist.

Lastly, another important parameter to look at is the wave impedance, which is described by:

$$Z_w(TE^z_{mn}) = \frac{E_x}{H_y} = \frac{E_y}{H_x} = \frac{\omega\mu}{\beta_z} \tag{12}$$

It is important to note that as frequency approaches the cutoff for a given mode, the wave impedance approaches infinity.

2.1.3 Cavity Modes

The field configuration within a cavity is very similar to a waveguide. TE or TM modes can exist and are derived in similar manner. Essentially, a cavity is a waveguide with conducting walls at each end. The main difference is that now additional boundary conditions are imposed and instead of a traveling wave in the z direction there is now another standing wave.

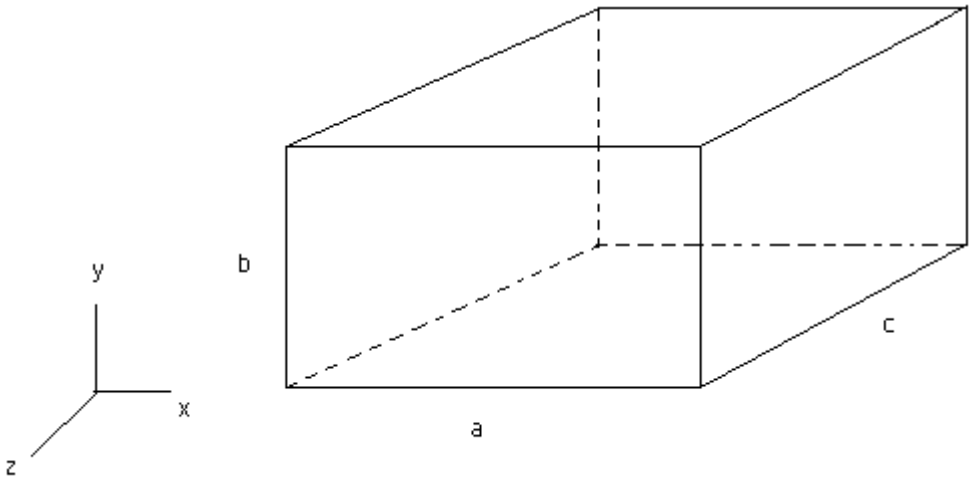

Figure 2.2: Cavity diagram, c > a > b

Recalling the general form for the fields within a waveguide, (3), the configuration within a cavity will have a very similar equation. Instead of assuming a traveling wave in the positive z direction, the $e^{-j\beta z}$ term is dropped and a standing wave is assumed.

$$F_Z(x,y,z) = [C_1\cos(\beta_x x) + D_1\sin(\beta_x x)]\big[C_2\cos(\beta_y y) + D_2\sin(\beta_y y)\big][C_3\cos(\beta_z z) + D_3\sin(\beta_z z)] \quad (13)$$

The separation equation (4) remains the same, but the additional boundary conditions are:

Condition 3 (Front and Back Walls):
$E_x(x, y, z = 0) = E_x(x, y, z = c) = 0$
$E_y(x, y, z = 0) = E_y(x, y, z = c) = 0$

Table 2-3: Additional Cavity Boundary Condition

Just as the waveguide example, applying Maxwell's curl equation and imposing the boundary conditions reduces (13) to

$$F_Z(x,y,z) = A_{mnp}\cos(\beta_x x)\cos(\beta_y y)\sin(\beta_z z) \tag{14}$$

With

$$\left.\begin{aligned} \beta_x &= \frac{m\pi}{a} \quad m = 0,1,2,\ldots \\ \beta_y &= \frac{n\pi}{b} \quad n = 0,1,2,\ldots \\ \beta_z &= \frac{p\pi}{c} \quad p = 1,2,3\ldots \end{aligned}\right\} m,n \neq 0\ simultaneously \tag{15}$$

Using (4) again to find the resonant frequency, and substituting the new value for β_z the resonant frequencies are found:

$$f_{mnp} = \frac{1}{2\pi\sqrt{\mu\varepsilon}}\sqrt{\left(\frac{m\pi}{a}\right)^2 + \left(\frac{n\pi}{b}\right)^2 + \left(\frac{p\pi}{c}\right)^2} \tag{16}$$

The wire mesh cage used in this thesis can be expected to behave like a cavity since it is a rectangular structure enclosed by conductive material. The first five expected modes for a solid walled cavity of the same dimensions as the animal cage are listed in Table 2-4 below.

Mode	Resonant Frequency
TE^z_{101}	650.21 MHz
TE^z_{011}	815.55 MHz
TM^z_{110}	816 MHz
TE^z_{111}	965.55 MHz
TE^z_{201}	1106.5 MHz

Table 2-4: Cavity Modes

The TE^z_{101} mode is the dominant mode, and lies within the frequency range of interest from 200-700 MHz. It is therefore expected that the mode will be excited. Below, Figure 2.3 displays the configuration of the TE^z_{101} mode. The dashed lines represent the $\vec{H}$ fields within the cavity. The magnetic fields circle around the perimeter as diagramed by the figure. They are weakest at the center of the cavity, and grow to their strongest near the walls. The $\vec{E}$ fields are

represented by the solid lines in Figure 2.3. The electric fields are weakest near the cavity walls and strongest at the center of the cage. The electric fields are uniform vertically.

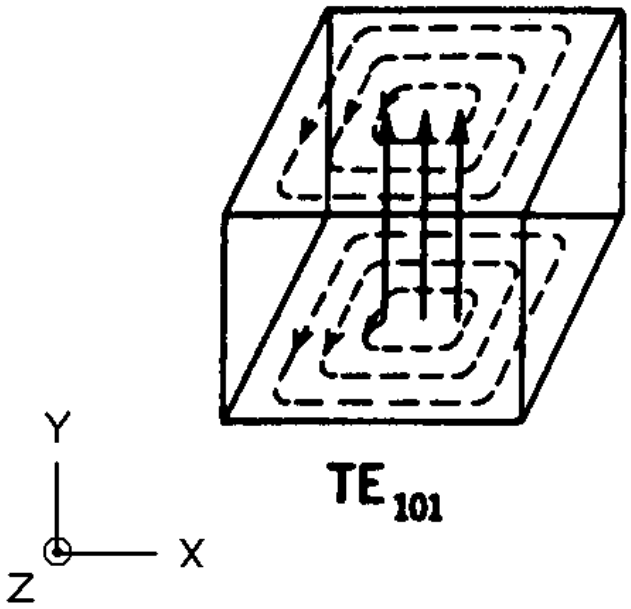

Figure 2.3: TE101 Mode Configuration

***Figure from Handbook of Microwave Technology: Volume 1, by T.K. Ishii.**

2.1.4 Quality Factor

The quality factor, Q, is defined as the ratio of energy stored in a band of frequencies to that of the energy lost in the same band during the time period of one cycle. Mathematically, it can be expressed as such:

$$Q = \omega \frac{stored\ energy}{dissipated\ energy} = \frac{f}{\Delta f} \tag{17}$$

Where f is the resonant frequency and Δf is the 3dB bandwidth. A low Q indicates a wide band of frequencies that can excite resonance, where a high Q is the opposite.

For a microwave cavity, typical Q values are between 5,000-10,000 [12]. This Q value is proportional to volume and inversely proportional to surface area. Energy is dissipated on the walls of the cavity, and stored in the fields. A low Q indicates a cavity's inability to store energy. This loss of energy can be through either dissipation due to ohmic resistance or leakage of electromagnetic fields through apertures and other openings. A high Q indicates a low loss cavity that can efficiently store energy.

The tradeoff between a low and high Q is demonstrated in Figure 2.4. As the Q decreases, the range of frequencies that can excite the mode increases. With a low Q it is possible to couple into a mode at much lower frequency than its resonance. While a high Q has a smaller range of frequencies that will couple to the resonance, more energy is stored at those frequencies.

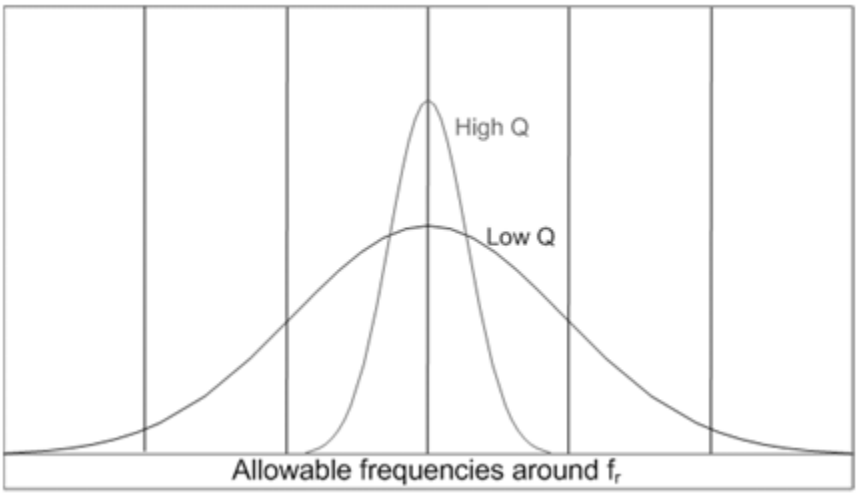

Figure 2.4: Quality Factor

By using the field expressions within a cavity, it is possible to estimate the Q. Referring to (17), the total stored energy and dissipated power can be estimated. The total stored energy from the electromagnetic fields within a cavity can be determined by a volume integral (18).

$$W = \left[\frac{\varepsilon}{2}\iiint_V |E|^2 dv\right] \tag{18}$$

The $\vec{E}$-fields come from the vector electric potential described by (14) substituted into Maxwell's curl equation (5). There is a unique Q value for each TE^z_{mnp} mode. The total dissipated energy can be found by adding up the energy that is dissipated on each wall of the cavity. The power dissipated on the top wall will be the same as that on the bottom, the right the same as the left, and the front the same as the back. This is shown below (19).

$$P_d = \frac{R_s}{2}\left[2\iint_{bottom} J_b \cdot J_b^* ds + 2\iint_{left} J_\ell \cdot J_\ell^* ds + 2\iint_{front} J_f \cdot J_f^* ds\right] \tag{19}$$

Where R_s is the surface resistivity and J_b, J_ℓ, and J_f, are current densities defined as:

$$\begin{aligned} J_b &= \hat{n} \times H_{y=0} \\ J_\ell &= \hat{n} \times H_{x=0} \\ J_f &= \hat{n} \times H_{c=z} \end{aligned} \tag{20}$$

The final value of the current densities and ultimately P_d depends on the mode being evaluated (same as for the total energy W). Once P_d and W have been solved, (17) will give an approximation to the Q of the enclosure, provided that R_s is known. In the case of this thesis, R_s represents the equivalent impedance of the mesh. The method outlined in this section is covered in [12]; equation (21) describes the Q of a cavity for the TE^z_{101} mode.

$$(Q)^{TE}_{101} = \frac{\pi\eta}{2R_s}\left[\frac{b(a^2+c^2)^{3/2}}{ac(a^2+c^2)+2b(a^3+c^3)}\right] \tag{21}$$

2.1.5 Wire Mesh Properties

A wire mesh is often used to provide shielding in place of a solid metal sheet. A mesh is cheaper, lighter, and also allows for air flow – which is particularly important for housing animals. The downside is its electromagnetic properties are more complex. At low frequencies, a planar mesh shield behaves in the same manner as a homogeneous metal shield of same material. As frequency increases however, attenuation remains constant until a point f_{min} where the shielding effect beings to decrease. For a range between f_{min} and some f_{max}, the attenuation of the mesh decreases until a point at which the mesh shield is completely transparent. The wavelength at this frequency is smaller than the size of the mesh. f_{min} and f_{max} are both determined by the properties of the mesh shield. A solid metal shield in comparison has an increasing shielding effect with frequency.

Casey in [7] develops a theory for mesh shields. Modeled by parallel sets of electrically connected wires with separation distance α, and diameter d, the surface impedance is characterized by

$$Z_s = R_s + j\omega L_s \qquad \Omega \tag{22}$$

With R_s and L_s defined as

$$R_s = \frac{4\alpha}{\pi d^2 \sigma} \frac{\sqrt{j\omega\tau_\omega} I_0\left(\sqrt{j\omega\tau_\omega}\right)}{2I_1\left(\sqrt{j\omega\tau_\omega}\right)} \tag{23}$$

$$L_s = \frac{u_0 \alpha}{2\pi} ln\left(\frac{1}{1 - e^{-\pi d/\alpha}}\right) \tag{24}$$

$I_0(\cdot)$ and $I_1(\cdot)$ are modified Bessel functions, σ is conductivity of the metal, μ is permeability, and τ_ω is the diffusion time in the wire given by

$$\tau_\omega = \frac{u_r \sigma d^2}{4} \tag{25}$$

Casey goes on to demonstrate the mesh impedance of a planar shield, deriving equations for f_{min} and f_{max}. Casey's results are summarized in [7] and generalizations for the shielding properties of a planar mesh shield and mesh enclosure in [14].

For the mesh cage used in this thesis it can be expected that as the frequency increases, the amount of leakage will increase. As the frequency increases towards resonance where maximum energy is stored, the cage's ability to contain the fields and prevent leakage through the mesh will decrease. This will substantially lower the Q of the cavity, allowing coupling to the mode at a lower frequency. This also leads to the idea that at some high frequency, the cage will no longer act as a cavity. However this will not happen until the wavelength is less than the size of the mesh [14], which does not occur until around 30GHz – far above the frequency range of interest from 200-700 MHz. Using (21) to calculate the Q of a cavity, (23) for R_s, and the values from Table 2-1, an estimate for the Q of the cage can be obtained. For the TE^z_{101} mode, the predicted Q is 68.7.

2.2 NEC Theory

2.2.1 NEC – Introduction

The Numerical Electromagnetics Code (NEC) is simulation software designed to solve radiation and scattering problems. Originally developed at Lawrence Livermore Laboratories for the military, NEC has evolved over the past 30 years and is available free to the public. NEC-2 is readily available and can be found on the internet along with many different user interfaces and post-processing codes. NEC-4 is restricted by the U.S. government but can be obtained with a license.

NEC is designed around the Method of Moments (MoM). Structures are modeled through a grid of wires. These wires are divided up into segments, and the induced current on each wire segment is solved for. The end points of each wire, and consequently each segment, are specified by the user; as well as the radius and conductivity. Very simple models from dipole antennas to more complex structures, such as helicopters, can be accurately built. NEC can compute the far field radiation patterns, current magnitudes, and near fields. For this thesis, near field simulation data is collected.

2.2.2 NEC – Method of Moments

The Method of Moments is used to calculate the current on each wire segment. It solves an integral equation, using sources specified by the user, and integrates using the Green's function to solve for the electric and magnetic fields. The integral equation is derived by first observing the relationship between the scattered field E_s and the vector magnetic potential A [18].

$$\vec{E}^s(\vec{r}) = -j\omega\vec{A} - \frac{j}{\omega\mu\varepsilon}\nabla(\nabla\cdot\vec{A}) \tag{26}$$

Where ω is the frequency in radians, μ is permeability, ε is permittivity, and $\vec{r}$ is a vector from the origin to an observation point. The vector magnetic potential, A, is related to the current density J_s on the surface of a conductor by:

$$\vec{A} = \int_S \vec{J}_s(\overrightarrow{r'})\frac{e^{-jk\left|\vec{r}-\overrightarrow{r'}\right|}}{\left|\vec{r}-\overrightarrow{r'}\right|}ds' \tag{27}$$

Where $\vec{r}'$ is a vector from the origin to the source, *s* is on the surface of the conductor, and *k* is the wave number defined as:

$$k = \omega\sqrt{\mu\varepsilon} \tag{28}$$

Substituting (27) into (26) yields:

$$\begin{aligned}\vec{E}^s(\vec{r}) = & -j\omega\mu\int_S \vec{J}_s(\vec{r}')\frac{e^{-jk|\vec{r}-\vec{r}'|}}{|\vec{r}-\vec{r}'|} \\ & + \frac{1}{j\omega\varepsilon}\nabla\int_S \nabla'\cdot\vec{J}_s(\vec{r}')\frac{e^{-jk|\vec{r}-\vec{r}'|}}{|\vec{r}-\vec{r}'|}\end{aligned} \tag{29}$$

The boundary condition that must be satisfied at the surface of a perfect conductor is:

$$\vec{E}_t^i + \vec{E}_t^s = 0 \tag{30}$$

Where E^i indicates the incident field and E^s is the scattered field. The *t* subscript denotes the tangential component of $\vec{E}$-field at the boundary.

NEC assumes thin and perfectly conducting wires. This allows for the current along each wire to be assumed in the axial direction only. The incident field, E^i is known, so the only remaining unknown is the current density J_s. Due to the assumption of current on the surface and in the axial direction, this allows J_s to be replaced by a current filament *I(s')* at wire location $\vec{r}'$. Where s' is a distance parameter along the wire axis at $\vec{r}'$. $\vec{s}$ is a unit vector tangent to the wire axis at $\vec{r}$. Evaluating the scattered electric field on the wire, (30) is used to write (29) as:

$$-\vec{s}\cdot\vec{E}^{i}(\vec{r}) = \frac{-j\eta}{4\pi k}\int_{L} I(s')\left[k^{2}\vec{s}\cdot\vec{s}' - \frac{\partial^{2}}{\partial s\partial s'}\right]\frac{e^{-jk|\vec{r}-\vec{r}'|}}{|\vec{r}-\vec{r}'|}d\ell' \quad (31)$$

The integral is over the entire collection, *L*, of wires and $d\ell'$ is a differential element along the wires. η is the intrinsic impedance. Equation (31) is known as the Electric Field Integral Equation (EFIE). NEC can also use the Magnetic Field Integral Equation (MFIE) for surface patches.

Equation (31) can be rewritten as a linear transformation:

$$L(f) = e \quad (32)$$

Where *e* represents the left hand side of (31), f is the unknown current $I(s')$, and *L* is the operator. f can then be written as a set of basis functions, f_i:

$$f(s') = \sum_{i=1}^{N} \alpha_i f_i(s') \quad (33)$$

Where α_i are the unknown constant coefficients and N is the number of segments. Substituting (33) into (32) will yield:

$$e = \sum_{i=1}^{N} \alpha_i L(f_i(s')) \quad (34)$$

With α_i still the only unknown. The basis functions used to approximate the total current on each segment are described by three terms. The first term is a constant, the second is a sine term, and the third is a cosine term.

$$f_i(s') = A_i + B_i \sin[2\pi(s' - s_i)/\lambda] + C_i \cos[2\pi(s' - s_i)/\lambda] \quad (35)$$

Where A_i, B_i, and C_i are the unknown coefficients, λ is wavelength, and s_i is the center of segment *s'*. Of the three unknowns, two are eliminated by local conditions . The last unknown is solved in a matrix equation.

Rewriting the system of linear equations in matrix form produces the following:

$$E = AZ \tag{36}$$

Where *E* is a vector containing the left hand side of (31), *A* is a vector of the unknown coefficients α_i, and *Z* is the matrix of $L(f_i(s'))$.

Since the f_i functions are known, *Z* can be computed and filled in. *Z* is known as the interaction matrix. This is because Z_{ij} is the scattered field at segment *i* due to the current on segment *j*. The wire specifications from the model define the size of *Z, N* segments in the model results in an *NxN* matrix. Z_{ij} is calculated by integrating (31) with the basis functions in (35).

The *E* vector requires knowledge of the incident field. This information is supplied by the excitation source in the model, which can be in the form of an antenna with an applied voltage or current, or as a plane wave.

The vector *A* is calculated by multiplying each side of the equation by the inverted *Z* matrix. This results in the current values on each of the *N* segments. After the currents are known, NEC proceeds to solve for the near or far fields.

2.2.3 NEC – Modeling Guidelines

NEC makes several important assumptions that can limit its accuracy. A standard list of guidelines to follow when modeling with NEC is below [18]:

- Wire segment length Δ should be less than 0.1λ and greater than 0.001λ;
- Wire radius, α, should be chosen so that 2πα/λ is much less than 1.0;
- The wire segment length Δ should be at least 8 times larger than the radius α;
- Wire segments with small Δ/α should be avoided at bends;
- Segments that are electrically connected must have coincident end points;
- Segments must not overlap;
- Large changes in radius between connected segments are to be avoided;

- Parallel wires should be several radii apart;
- Connected segments that have a small angle between them are to be avoided;

Since NEC uses the Method of Moments to solve the integral equation, the wires are divided into short straight segments with a sample point at the center of each. The basis functions used to approximate the total current on each segment are described by three terms from (35). If a segment is too small in relation to wavelength, the constant and cosine terms in the basis functions become equivalent on the segments resulting in erroneous data. Junctions with largely unequal radii of segments should be avoided because a generalization is made from the continuity of current and charge to Kirchhoff's current law to solve for the unknowns. Junctions of unequal radii decrease accuracy. Since NEC uses continuity conditions at the ends of the segments to solve for the coefficients of the basis functions, segments that are electrically connected must have coincident end points. In addition, segments cannot overlap as this can result in an extremely small $|\vec{r} - \vec{r}'|$ term in (31) causing the kernel to become very large. For a similar reason, parallel wires in close proximity are also to be avoided.

To solve for the interaction matrix Z, NEC must use approximations for the integral equation kernel. There are three different approximations available to the code: a thin-wire form, an extended thin-wire for thick wires, and a current element approximation for large distances. The accuracy of the thin-wire form depends on the radius of the wire and segment length in relation to the wavelength. [19] shows errors of less than 1% can be expected for a segment length greater than eight times the radius, and wires should be divided in segments of less than 0.1λ in length to obtain an accurate representation of the current distribution.

The guidelines given above are not unbreakable rules. They are simply the most common sources of error in NEC, it is possible to generate inaccurate data due to other

conditions. It is also possible to "bend" the rules as long as the user is aware and checking the output for errors.

2.2.4 NEC – Animal Cage Model

The NEC model of the cage was built to resemble the actual cage as closely as possible. The wire diameter was set to 1mm. Each square in the mesh is approximately 1.2 cm by 1.2 cm with a total of about 6500 segments in the model. Figure 2.5 through Figure 2.9 show the NEC model from different angles. It should be noted that one of the guidelines listed in the previous section is not completely obeyed. The lowest simulation frequency the model ran at was 200 MHz, which has a wavelength of 1.5m. This means the smallest segment should be no less than 1.5cm. However, the average size segment in the model is 1.2cm. Along the top and bottom of the cage (Figure 2.6) there are several segments only 0.95cm in length. This violation of the guidelines did not appear to affect results. In addition, once the frequency was above 300 MHz, none of the segments were less than the length suggested by the guidelines. All other conditions set forth by the guidelines were met.

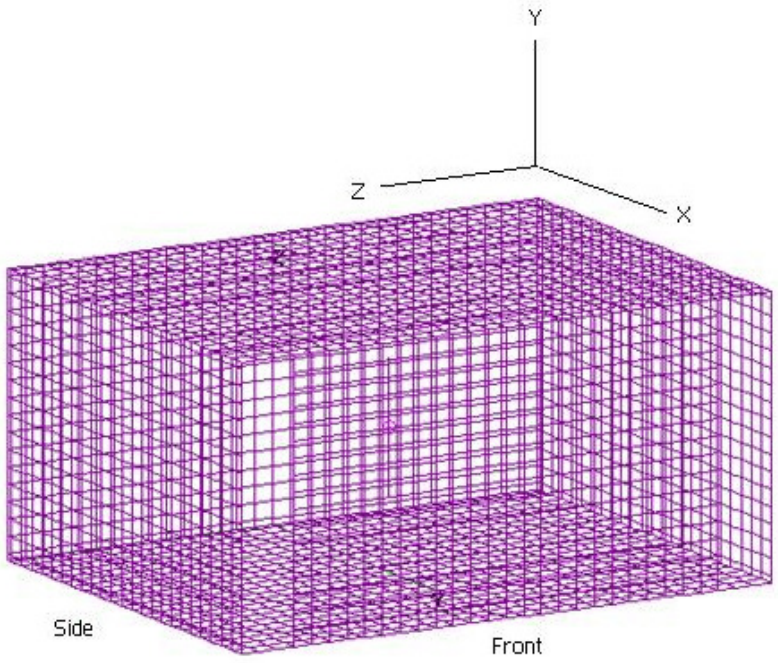

Figure 2.5: 3D View of Cage

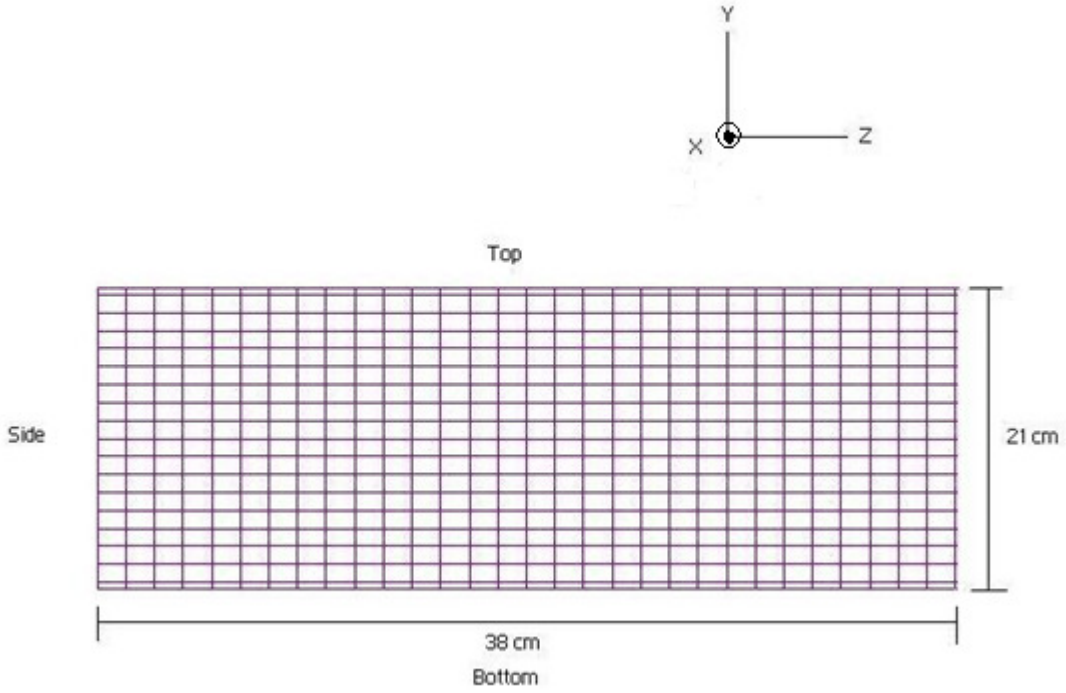

Figure 2.6: Back of Cage

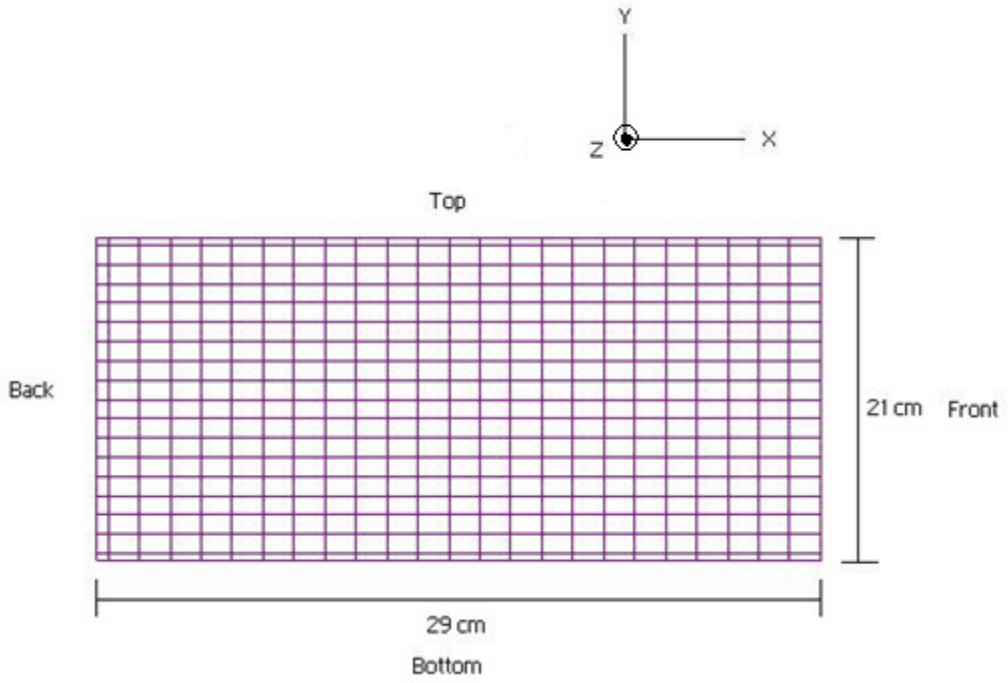

Figure 2.7: Side View of Cage

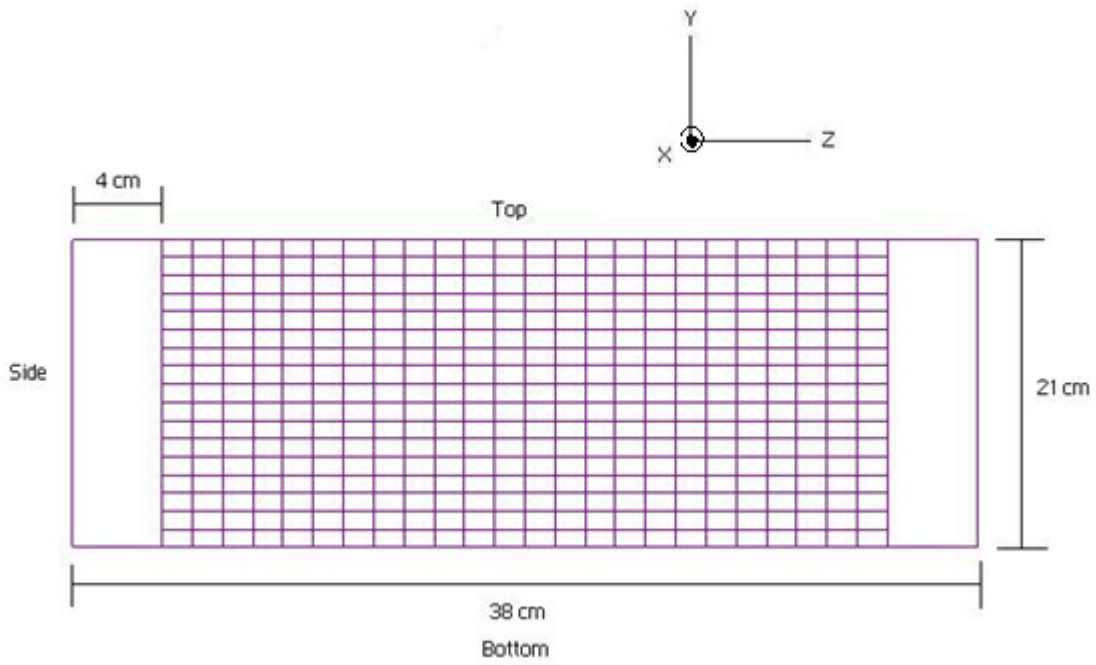

Figure 2.8: Front of Cage

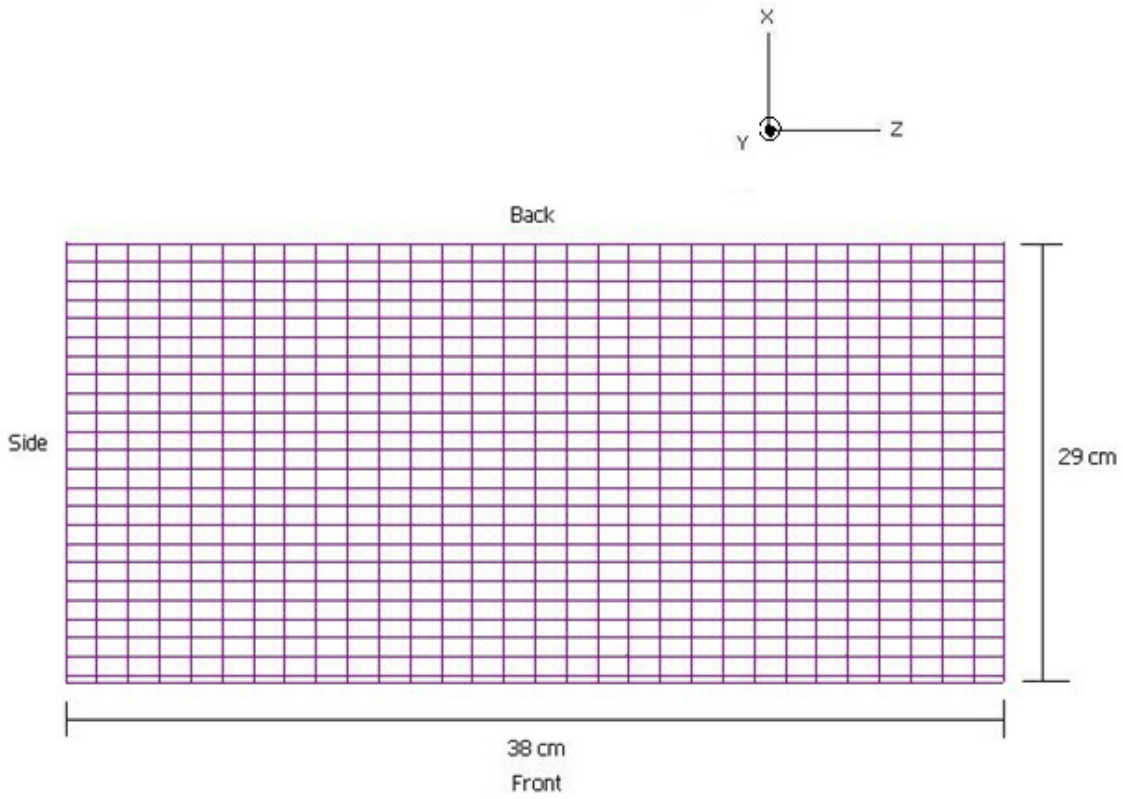

Figure 2.9: Top View of Cage

2.3 NEC Simulation Setup

2.3.1 Antenna Theory

Three types of antennas were used for simulations; dipole, monopole, and loop. For experiments, only monopole and loops were used. The dipole was used because of its simplicity, and ability to excite the $\vec{E}$-fields within the cage. The loop was used because it is a magnetic antenna, and well suited to excite the $\vec{H}$-fields. The monopole was used as a replacement for the dipole in experiments. It would have been difficult to build and use a dipole antenna experimentally because it requires a balun. Consequently, the dipole was only used for simulations to help gain an understanding of how the fields within the cage were acting. The monopole is a suitable replacement due to its many similarities to the dipole.

A center fed dipole will have a current distribution along its length. This distribution is strongest in magnitude at the center, and goes to zero and is opposite in polarity at the ends. This results in radiated fields, with dominant $\vec{E}$-fields parallel to the direction of current flow and the dominant H-fields perpendicular (see Figure 2.10). Since the strongest E-fields created by the dipole are in the axial direction, to couple to a cavity it should be orientated in the same direction as the $\vec{E}$-fields described by the mode configuration.

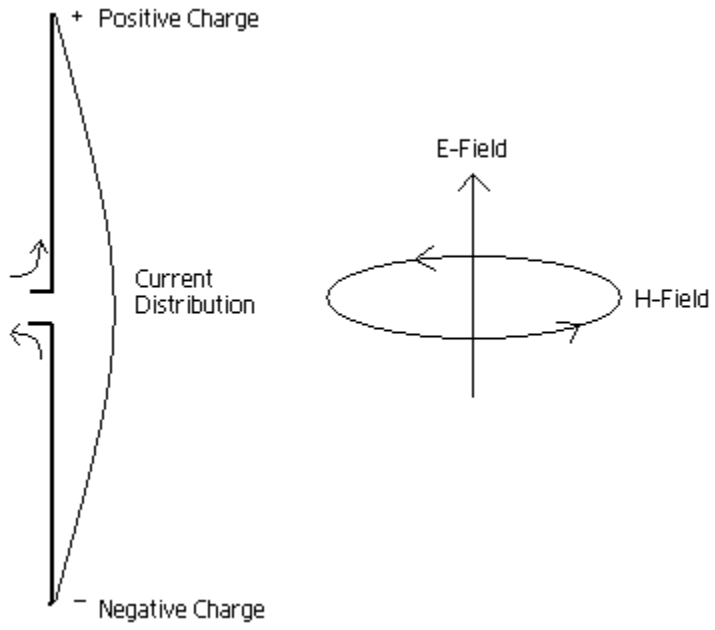

Figure 2.10: Dipole Antenna

The monopole antenna can be used as a replacement to the dipole because it is very similar. The monopole can be understood using image theory. Essentially one half of the dipole is replaced with a ground plane, if large enough this will create a theoretical mirror image of the missing bottom half. Just like the dipole, the dominant $\vec{E}$-fields are parallel to the antenna, and the $\vec{H}$-fields are perpendicular.

While the dipole and monopole antennas are effective for exciting the $\vec{E}$-fields within a cavity; a small loop antenna is effective for exciting the magnetic fields. With a circumference of less than 1/10λ, the current can be considered constant around the loop. The current traveling through the wire of the loop generates an $\vec{H}$-field that curls around the wire and a perpendicular $\vec{E}$-field. See Figure 2.11.

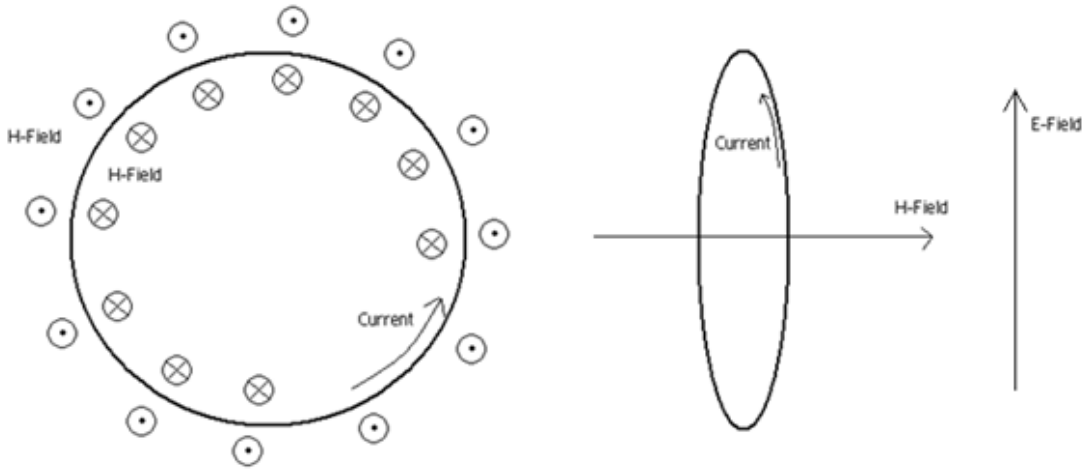

Figure 2.11: Loop Antenna

2.3.2 Antenna Locations and Orientations

The antennas were simulated in NEC at various positions within the cage. The position of the antenna was determined by its ability to couple to the nearest mode. Since TE_{101}^{z} was the dominant mode, antenna orientation was set up to excite the TE_{101}^{z} mode.

Four positions were used for the dipole, shown in Figure 2.12. Position A is the point of maximum field strength within the cage, as suggested by the configuration of the TE_{101}^{z} mode. So, it should be the best spot to excite the mode. Positions B and C are near the edges of the cage. Due to the electromagnetic properties of a cavity, the fields must go to zero as they approach the sides. Positions B and C should couple weakly to the TE_{101}^{z} mode. Position D is in the corner of the cage near the aperture opening. This should be the worst point to couple into the TE_{101}^{z} mode. Not only is the dipole in a corner where the fields must go to zero but it is also near an aperture where additional leakage will occur.

For Figure 2.12 the dipole is positioned vertically, coming out of the page. In Figure 2.13, the monopole is mounted to the top of the cage extending downwards. In Figure 2.14 the dot indicates the loop antenna, orientated such that cross section is perpendicular to the page.

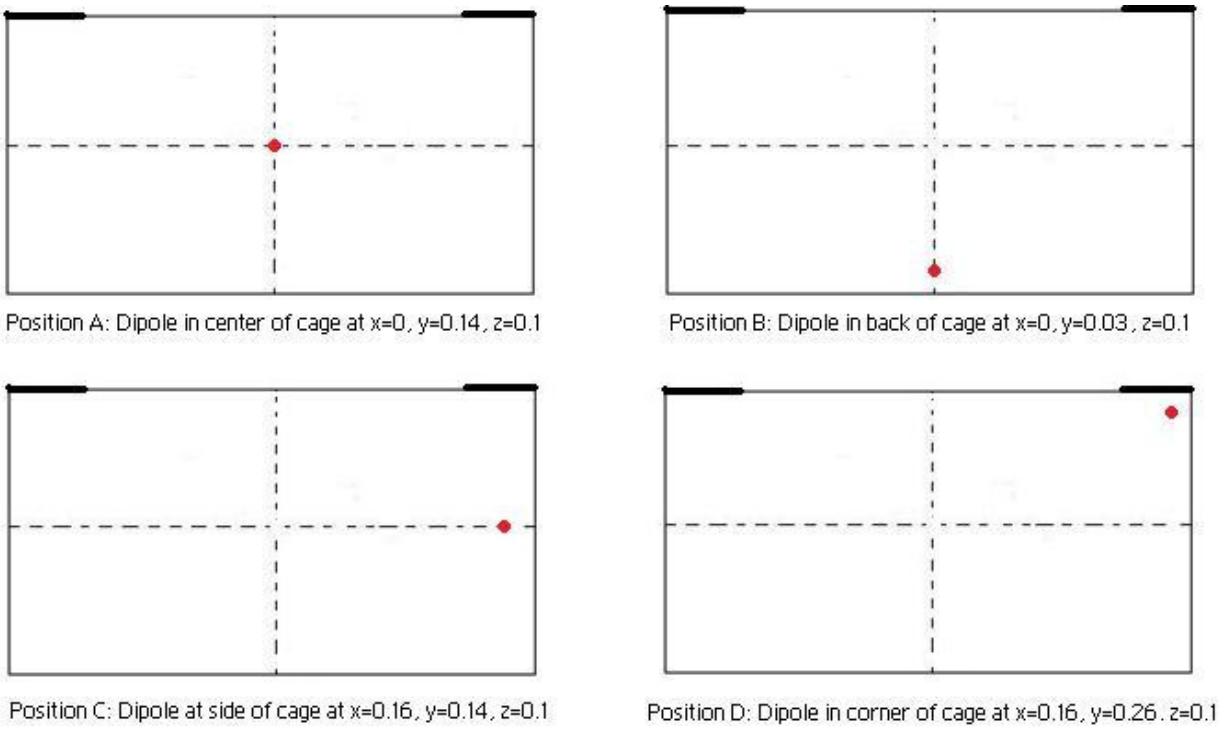

Figure 2.12: Dipole Antenna Positions

The cage walls were used as the ground plane for the monopole antenna in the NEC model. The locations were the same as the dipole, except for a change in height.

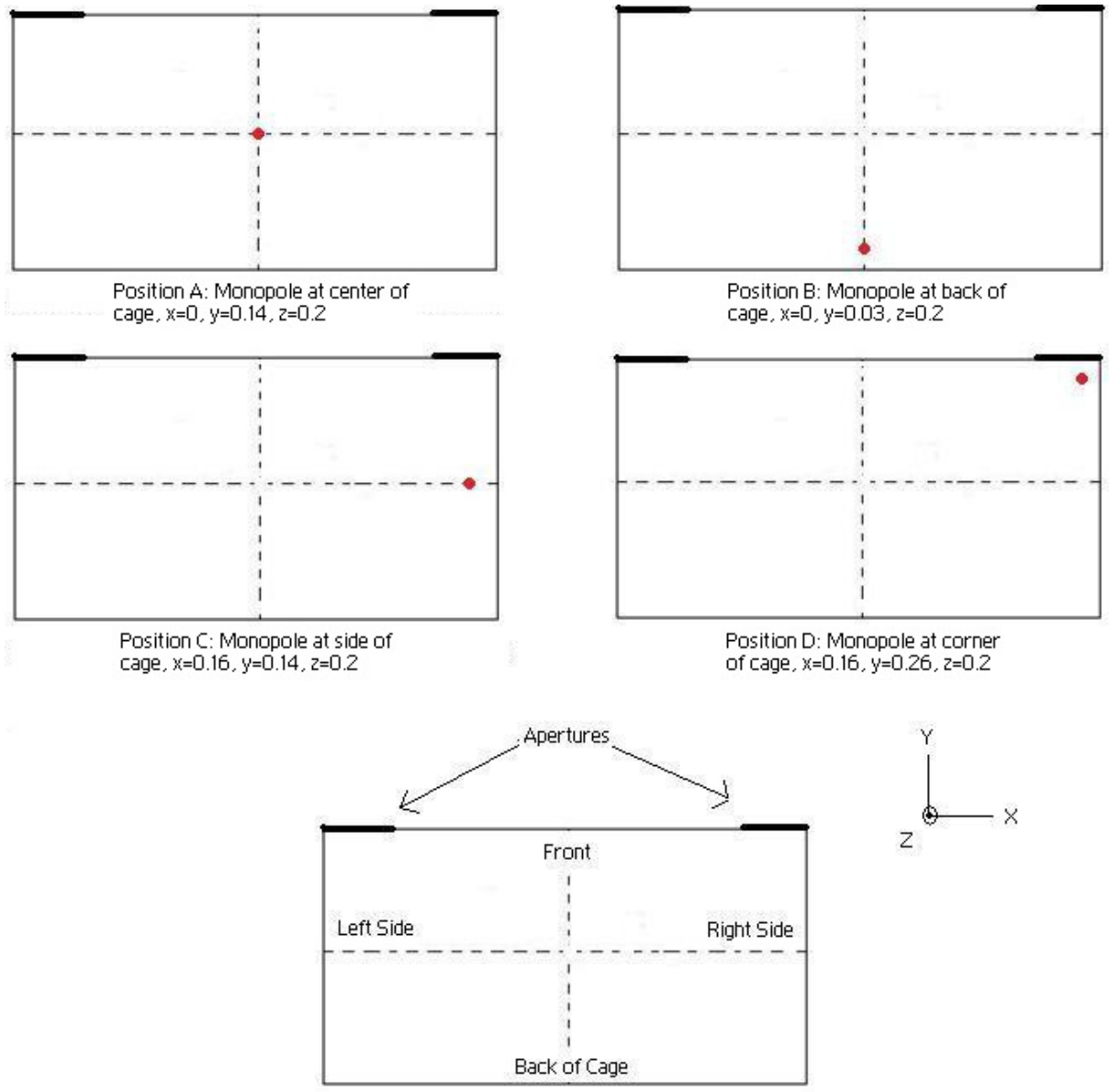

Figure 2.13: Monopole Antenna Positions

For the loop antennas, three positions were evaluated. Since the loop antenna is magnetic, it should be placed where the $\vec{H}$-fields are strongest. The configuration of the TE_{101}^{z} mode suggests strong $\vec{H}$-fields will be present at the edges of the cage, where the $\vec{E}$-fields are weakest. Position A and B are both at the edges and should excite the mode well. Position C is at the center of the cage, here the $\vec{E}$-fields are strongest and the $\vec{H}$-fields weakest. The loop is orientated with its cross section perpendicular to the page.

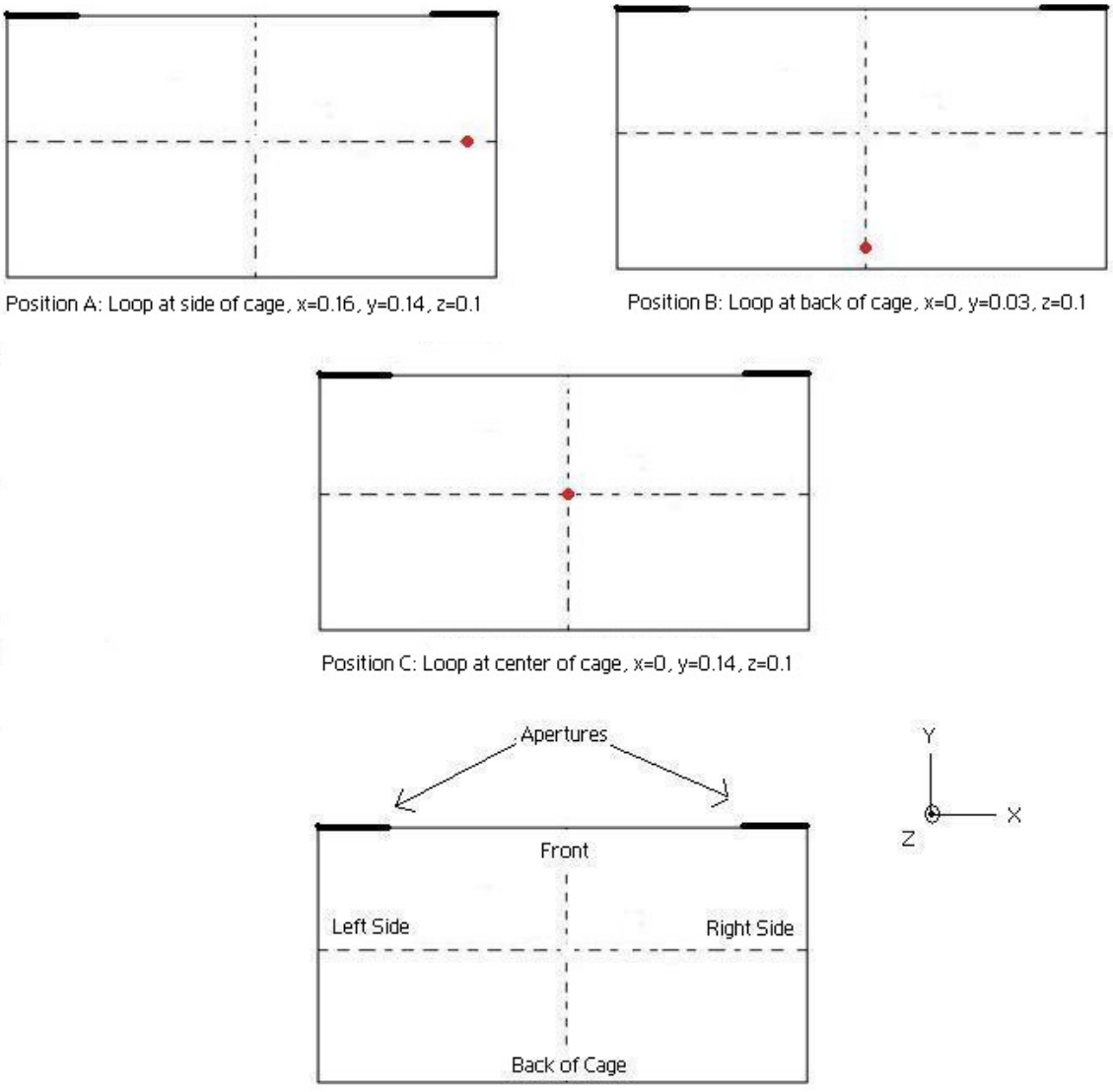

Figure 2.14: Loop Antenna Positions

2.3.3 Frequency Range

The original problem formulation from Dr. Jeutter investigated the electromagnetic field configuration within the animal cage at 200 MHz. This was later expanded to a range of frequencies, starting at 200 MHz up to 700 MHz. It was decided to include the ISM band at 433 MHz and the first resonant mode at 650MHz. Simulation data was gathered from NEC at 10MHz increments. Table 2-5 is a brief list of frequencies and their wavelength.

Frequency (MHz)	Wavelength (m)
200	1.5000
250	1.2000
300	1.0000
350	0.8571
400	0.7500
450	0.6667
500	0.6000
550	0.5455
600	0.5000
650	0.4615
700	0.4286

Table 2-5: Frequency Range Wavelengths

3 Experimental Setup

3.1 Matlab Post-Processing

Matlab was used for processing the output file produced by the NEC engine. Each simulation was normalized in order to compare it to other simulations. Since NEC uses a 1 volt excitation source, and changing frequency results in a change of input impedance, each simulation had a different input power. This made it difficult to compare results. Additionally, data was being analyzed in the near field of the antenna. Energy was not being radiated, but stored instead in the reactive fields. This made it difficult to scale each simulation according to its input power since the amount of energy being stored and radiated constantly changed. In order to make the data easily comparable, the near $\vec{E}$ field data was normalized to the maximum $\vec{E}$ field value in each simulation. All contour plots shown in this thesis are normalized in this manner. The y-scale of each contour plot is in dB (37), and indicates a point's strength in decibels with respect to the max $\vec{E}$ field value at that particular frequency. Additionally, all line graphs that plot field strength are normalized in the same manner. Graphs of input impedance are not normalized.

$$E(dB) = 20 * log_{10} \frac{\left|\vec{E}(\vec{r})\right|}{\left|\vec{E}_{max}\right|} \quad (3$$

3.2 Antenna Design

Two sets of monopole antennas were designed, one was electrically small and the other was not. For an antenna to be considered electrically small, it must have a maximum dimension of λ/10 [21]. A 4cm dipole and 2cm monopole where used in NEC simulations. From Table 2-5, it can be seen that these dimensions satisfy the condition to be electrically small. For the larger antenna set, 10cm dipoles and 8cm monopoles were used for NEC simulations. Experimentally, 8 and 4cm monopoles were used.

For the loop antenna, only one antenna size was investigated. A 3x3cm square was used in NEC and a 3cm diameter loop for experiments. Loop antennas are judged by their circumference, and not diameter. A 3cm square loop has a perimeter length of 12cm.

RG-188U coaxial cable was used to make the experimental antennas. For the monopole, the outer conductor was stripped back and soldered to a copper ground plane. For the loop, the insulation was stripped off and the end of the cable curled back and soldered to the outer conductor. Exactly opposite, the cable was cut and the inner conductor soldered to the outer, see Figure 3.1.

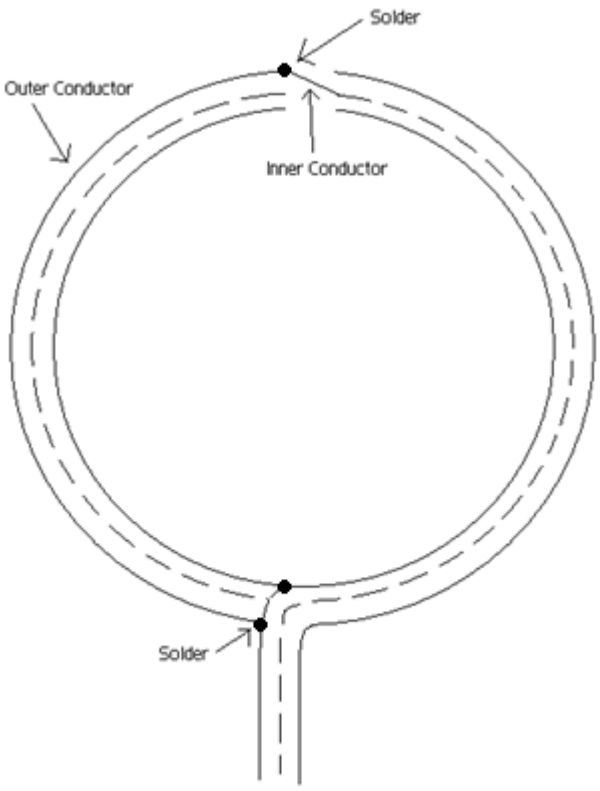

Figure 3.1: Loop Diagram

3.3 Experimental Setup

Experiments were carried out in the RF/Wireless Laboratory at Marquette University. A vector network analyzer (Agilent 8714 ES) was used to gather data. The VNA was calibrated with 50-Ohm coaxial cable leads from 200 MHz to 700 MHz. Due to small inaccuracies in the calibration process, a small amount error may have been introduced in some measurements. After calibration, monopole antennas were setup up corresponding to Figure 2.13, and Figure 2.14 for loops. S_{11} and input impedance were measured. At each position, S_{21} was also measured at the locations shown in Figure 3.2 for the monopole and Figure 3.3 for the loop. Since the antennas are reciprocal devices, results were not affected by which antenna was transmitting and which was receiving.

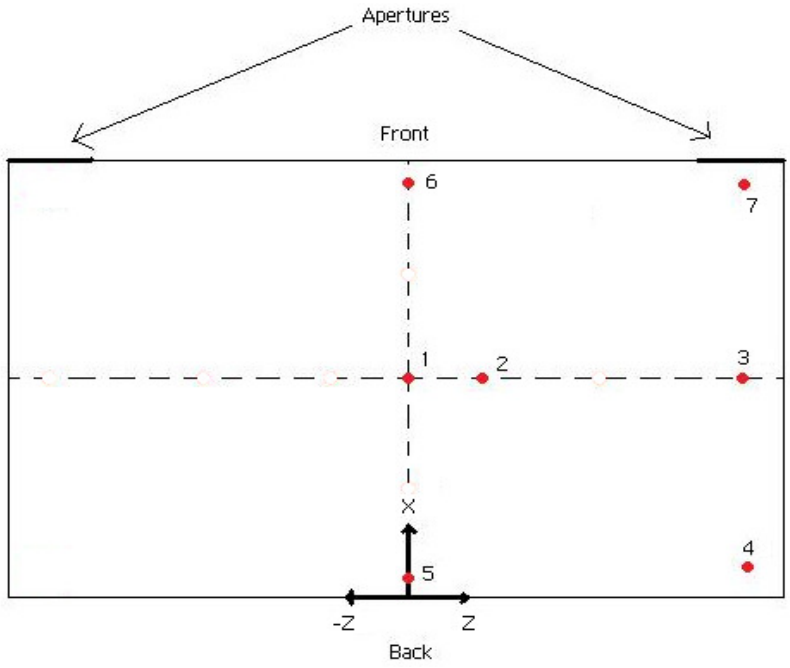

Figure 3.2: S21 Monopole Measurement Locations

Position	Coordinates (cm)
1	Z=0, X=14
2	Z=5, X=14
3	Z=16, X=14
4	Z=16, X=3
5	Z=0, X=3
6	Z=0, X=26
7	Z=16, X=26

Table 3-1: S21 Monopole Measurement Coordinates

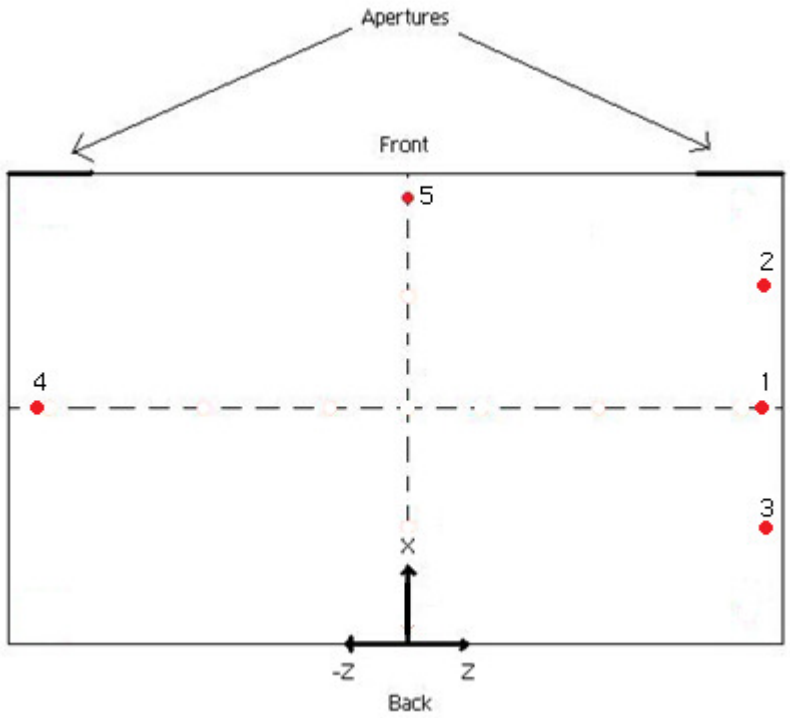

Figure 3.3: S21 Loop Measurement Locations

Position	Coordinates (cm)
1	Z=18, X=14
2	Z=18, X=18
3	Z=18, X=9
4	Z=-18, X=14
5	Z=0, X=28

Table 3-2: S21 Loop Measurement Locations

A solid metal box of same dimensions as the mesh cage was constructed out of printed circuit boards (PCBs). The PCB boarding created a solid walled cavity, resulting in a high Q environment. This created a comparison to the wire mesh cage, which was also a cavity but had a very low Q. The two different extremes allowed for a comparison as to how the antennas would behave differently as the Q changed. Since both enclosures were acting as cavities and had the same dimensions, performing the same antenna measurements yielded results that were predominately only affected by the change in Q.

4 Simulated Dipole Results

This chapter will demonstrate the behavior and performance of a dipole placed inside the animal cage. All data presented is from NEC simulation results, no experimental data is given here. This chapter will provide basic information regarding antenna input impedance, size, location and current distribution, as well as modal development and field configuration within the animal cage. Ultimately, the results will be used as a foundation for conclusions for the monopole in Chapter 6 and the loop in Chapter 7.

Two types of contour plots are shown in this chapter. The red line in Figure 4.1 shows where the plane for contour plots of Y=10cm is, and the blue line in Figure 4.2 for X=14cm.

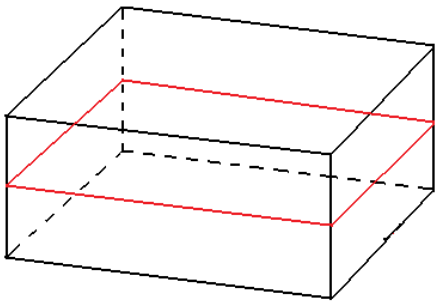

Figure 4.1: Plane of Contour Plots at Y=10cm

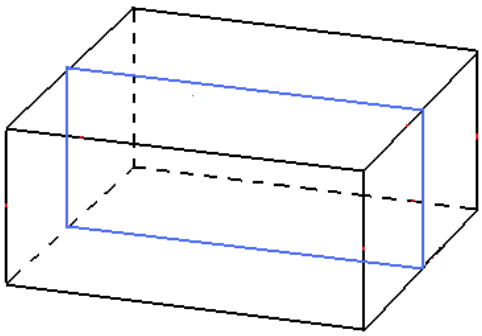

Figure 4.2: Plane of Contour Plots at X=14cm

4.1 Electrically Small 4cm Dipole

A 4cm, electrically small dipole was used to obtain a basic understanding of how the electromagnetic fields were acting within the cage. The dipole will be placed in the center of the cage and examined at three frequencies, 200 MHz, 433 MHz, and resonance at 634 MHz. This section will show the development of the TE_{101}^{z} mode and a null around the antenna at frequencies below resonance. Additionally, large changes in the antenna input impedance will be discussed.

Figure 4.3 is a contour plot of Ey field strength at 200MHz within the cage cut at a height of Y=10cm (see Figure 4.1). Figure 4.4 is a line plot of the Ey field strength also at a height of Y=10cm along the Z-axis. Inspection of the two figures shows that the fields are evanescent within the cage and quickly decrease away from the source. This is expected for a cavity below cutoff.

As the frequency is increased, coupling to the first resonant mode begins. Figure 4.5 is contour plot of Ey field strength at 433 MHz. Prominently displayed, a null has formed around the antenna. Figure 4.6 shows this null and the developing mode more clearly. Since the frequency is still below cutoff, near the antenna the fields are rapidly decreasing in magnitude. Near the edges of the cage though, the TE_{101}^{z} mode is beginning to develop. The sinusoidal shape that defines the mode is beginning to show. The null seen in Figure 4.5 is evidenced by the two sharp drops at Z = ± 9cm, at which the reflected fields from the cage walls are out of phase with the near fields of the antenna. Figure 4.7 is a contour plot of the Ey field strength cut in the X-plane at X=14cm, showing a vertical view of the Ey fields from top to bottom of the cage. This shows that the null is centered on the middle of the antenna and has a sphere like shape.

Once the cage has reached resonance, a number of effects can be seen. Figure 4.8 is a contour plot of the Ey field distribution at resonance of 634 MHz. The fields within the cage are extremely strong and distributed as expected per the TE_{101}^{Z} mode. In addition, there is considerably more leakage compared to previous contour plots at 200 MHz and 433 MHz (Figure 4.3 and Figure 4.5). Figure 4.9 demonstrates the sinusoidal nature of the $\vec{E}$ field distribution within the animal cage. The slight dip in the center is due to the presence of the antenna. Mathematical resonance was predicted to be 650MHz, but NEC simulations show it to be 634 MHz. The inability of the mesh to act as a solid conductor lowers the resonant frequency. The $\vec{E}$ field does not completely go to zero at the cavity walls; it drops significantly at the mesh but extends out just past the cage wall. This effect causes a lower resonant frequency at a wavelength slightly greater than the dimensions of the cage to exist. At resonance, the $\vec{E}$ fields within the cage appear to be behaving as expected from the configuration of the TE_{101}^{Z} mode, with the effect of the wire-mesh cage limited to simply lowering the cutoff frequency to 634 MHz.

Figure 4.10 and Figure 4.11 are plots of the Ey field strength at two different locations over the entire frequency range from 200-700MHz. The Ey field strength is much less in Figure 4.11, which is a result of the sampling point being very close to the edge of the cage where the $\vec{E}$ fields sharply decrease to satisfy boundary conditions. Comparing the two figures also shows that both sampling locations exhibit a null but at different frequencies. The null appears to start at the edges of the cage and move towards the antenna as frequency increases. The null signifies an area where the reflected Ey fields coming from the cage walls are destructively interfering with the Ey fields radiating from the dipole. This is further demonstrated in Figure 4.12, as the frequency increases the modal fields grow and the region of near electric fields

shrinks. The null position continues to shrink until it reaches the antenna and disappears at cage resonance.

Figure 4.13 and Figure 4.14 are plots of the real and reactive input impedances of the antenna. By examination of the two figures, the electrically small 4cm dipole exhibits a sharp impedance increase at cavity resonance. Once placed inside, the antenna is now a function of the cavity. At resonance the reflected fields within the cage are interacting with the antenna and inducing currents on the dipole. This causes the dipole input impedance to change according to the new currents forced on it.

In summary, this section has demonstrated that first resonant mode exists in the wire-mesh animal cage. Along with the mode, a frequency dependent null appears as a result of destructive interference between the reflected fields and radiated fields from the antenna. Lastly, it was shown that an antenna's input impedance changes as the cavity approaches resonance.

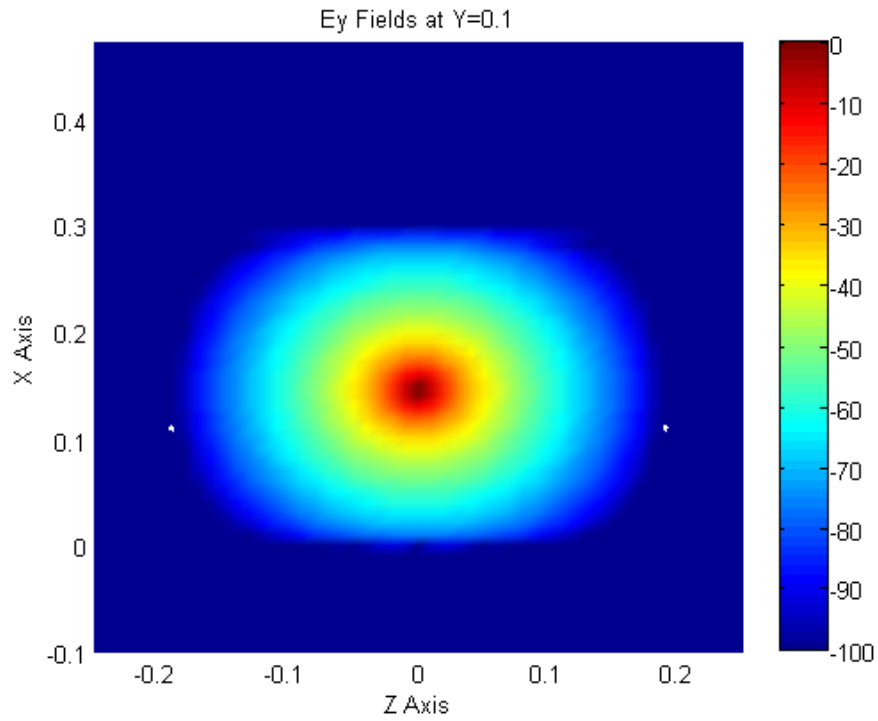

Figure 4.3: 4cm Ey Field Distribution at 200 MHz, dB

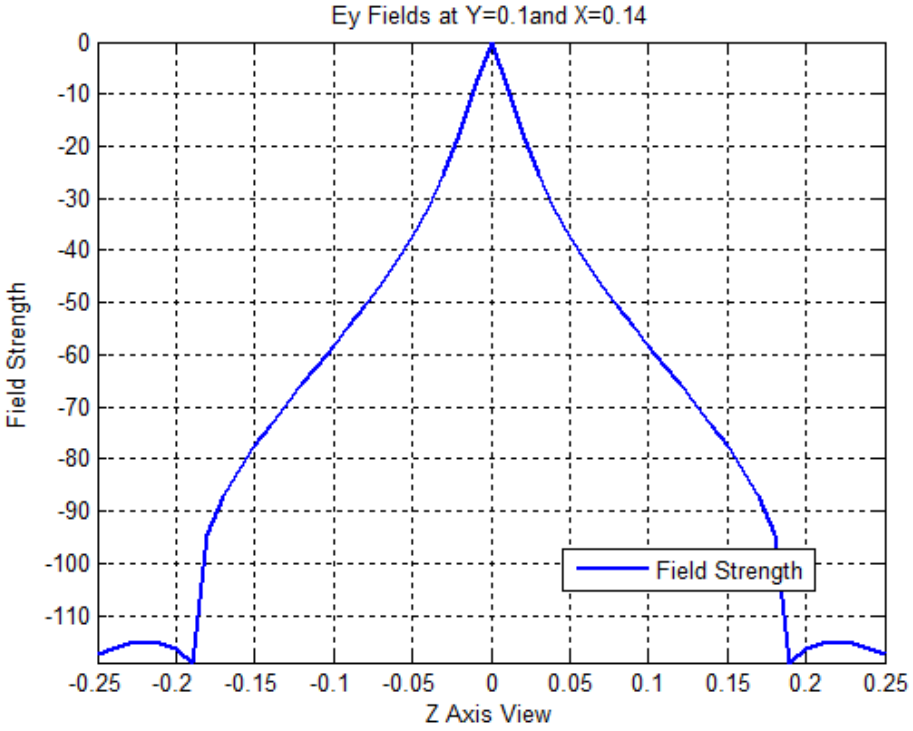

Figure 4.4: 4cm Ey Field Strength at 200 MHz, dB

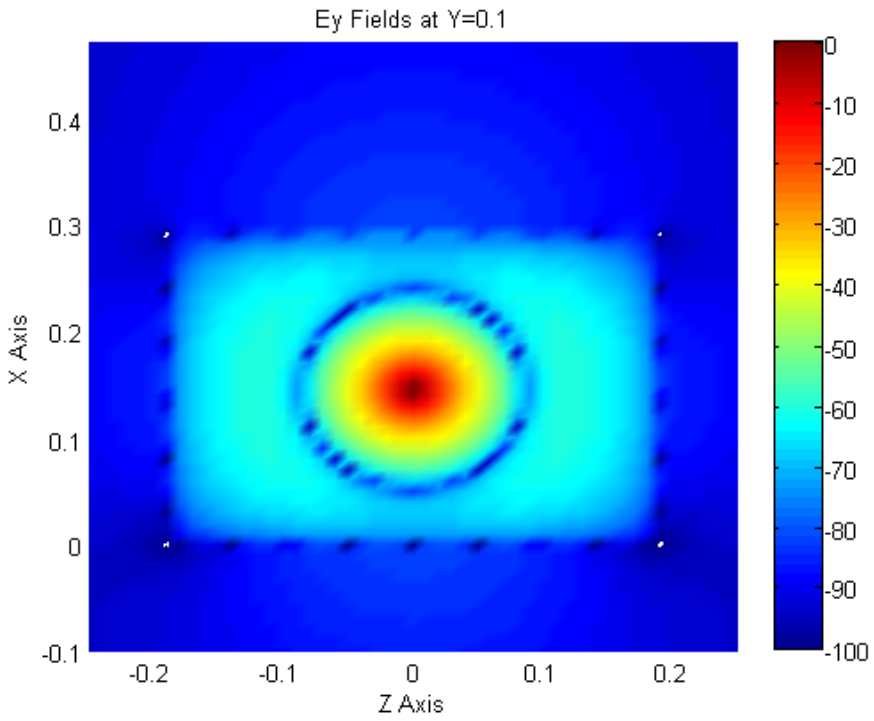

Figure 4.5: Ey Field Distribution at 433 MHz, dB

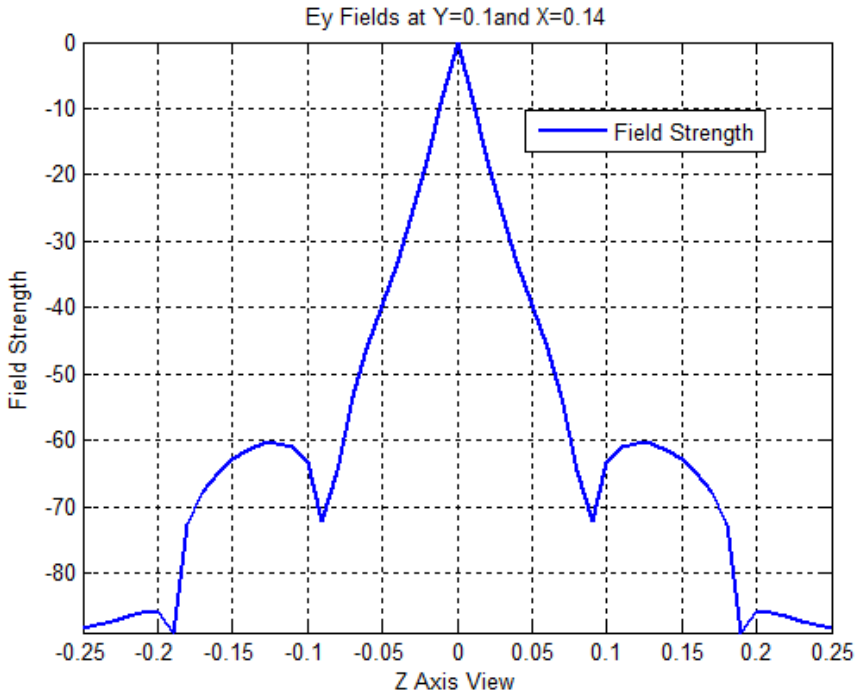

Figure 4.6: Ey Field Strength at 433 MHz, dB

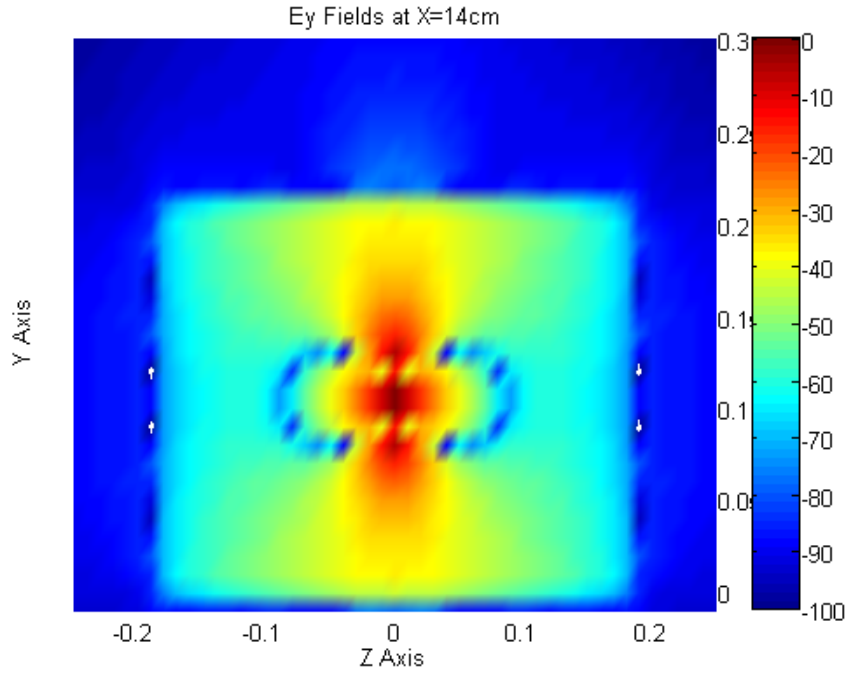

Figure 4.7: Contour plot Ey field strength cut in X-plane at 433MHz, dB

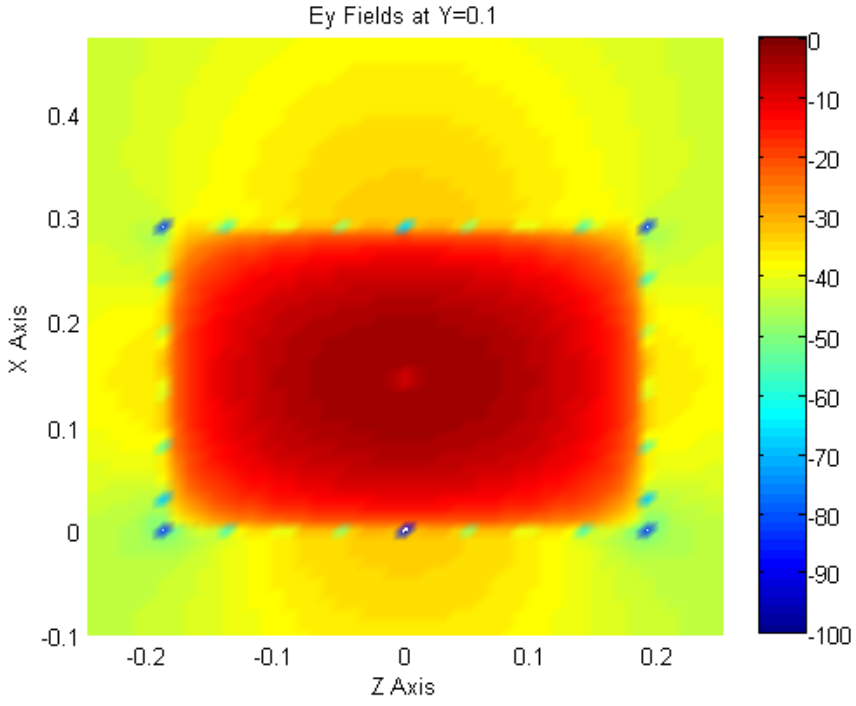

Figure 4.8: Ey Field Distribution at 634 MHz, dB

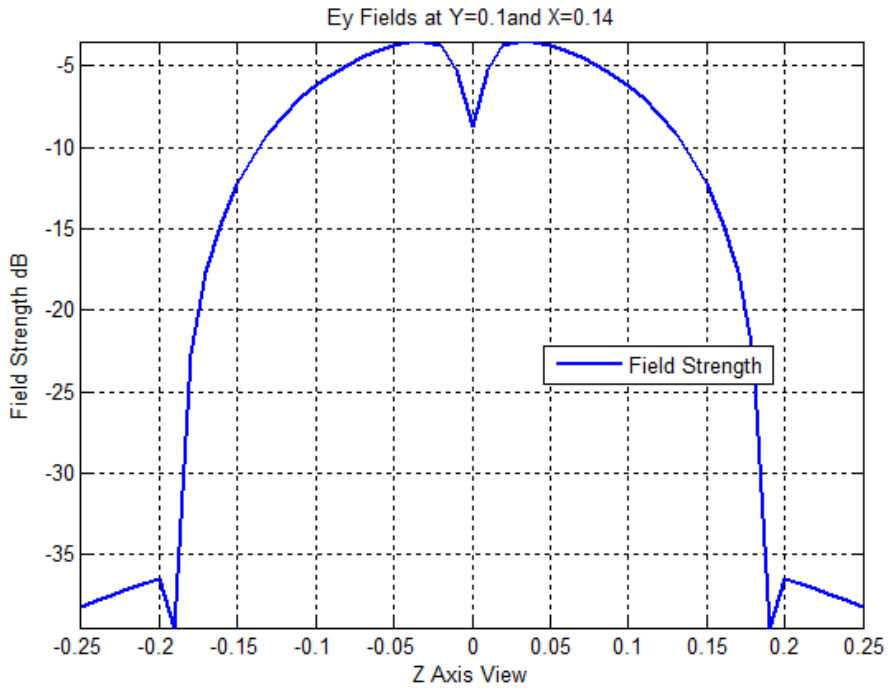

Figure 4.9: Ey Field Strength at 634 MHz

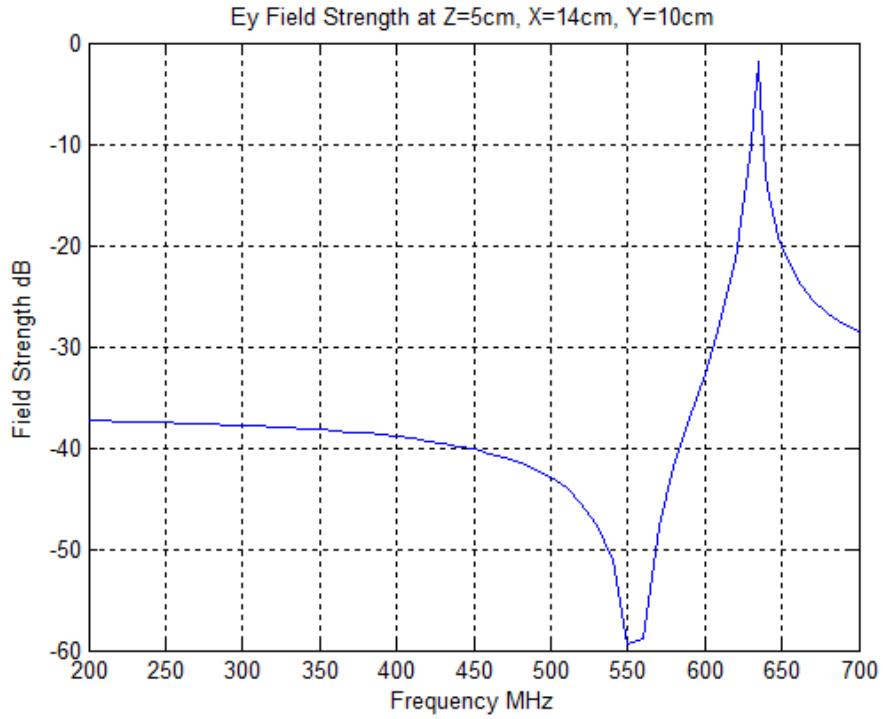

Figure 4.10: Ey Field Strength Trend at X=5cm

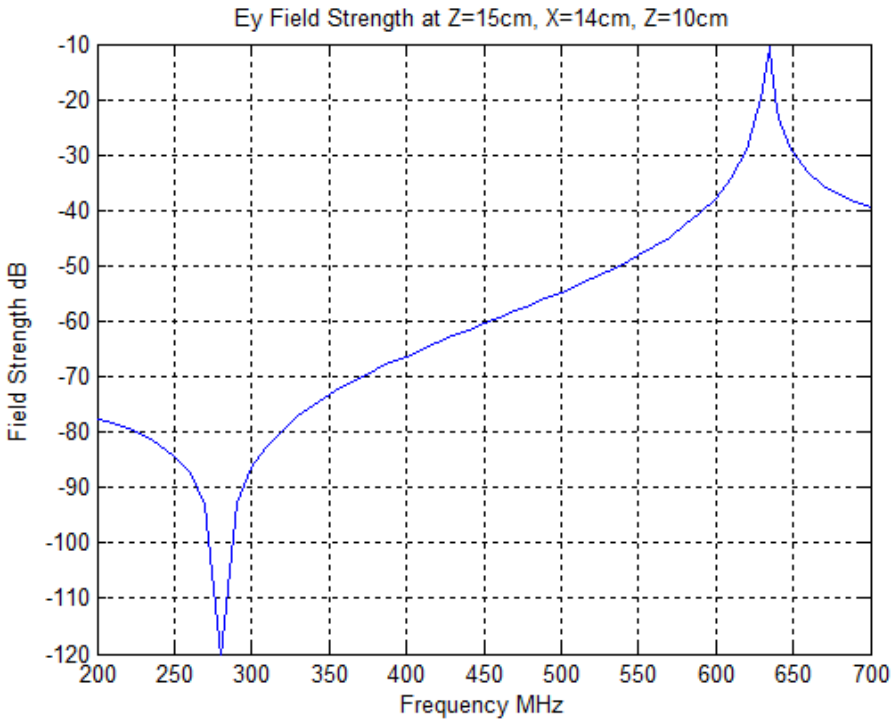

Figure 4.11: Ey Field Strength Trend at X=15cm

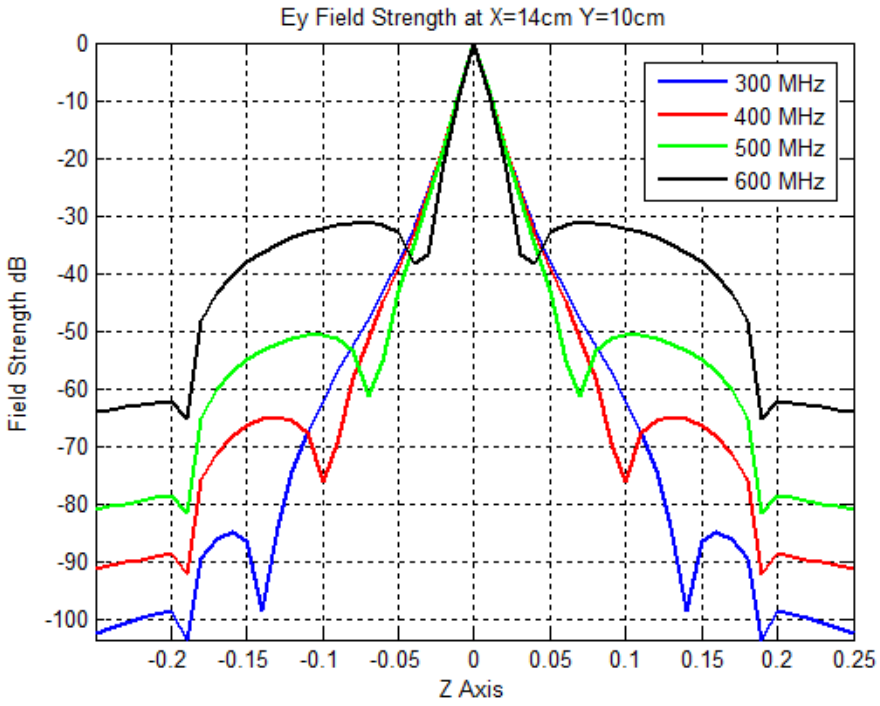

Figure 4.12: Ey Field Strength at 300, 400, 500, and 600 MHz

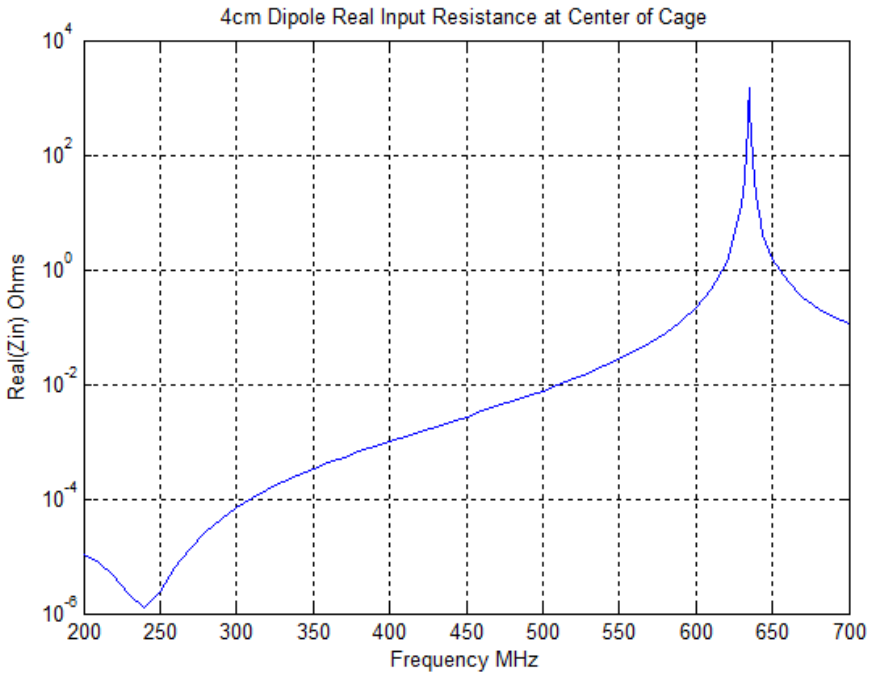

Figure 4.13: Real(Zin) of Antenna

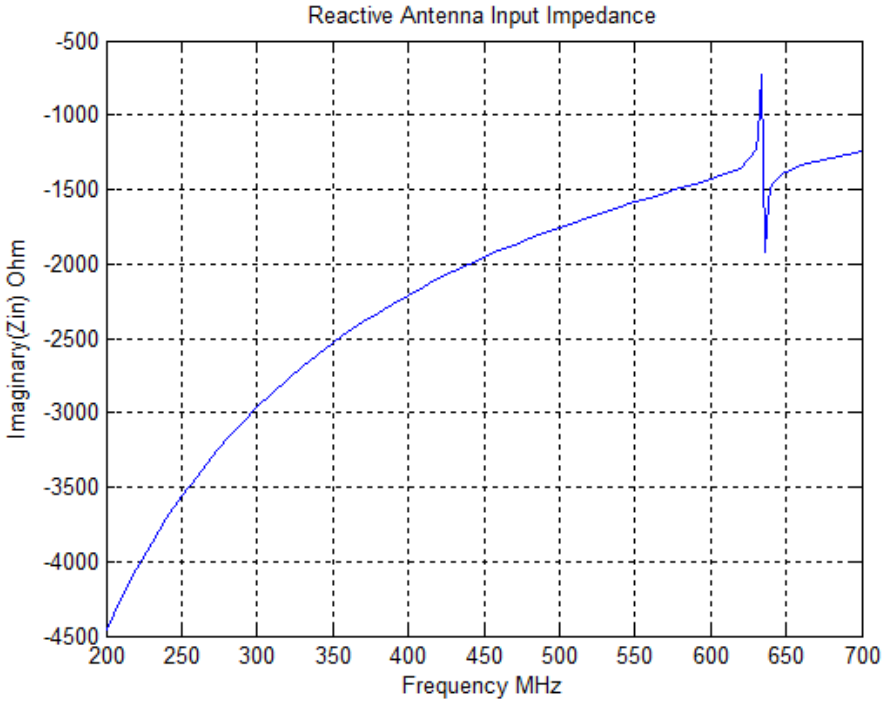

Figure 4.14: Imaginary(Zin) of Antenna

4.2 10cm Dipole Simulation Results

A 10cm dipole was simulated to see the effect antenna size with regard to wavelength would have on the field distribution. At low frequencies, 10cm is electrically small, but at 700 MHz the antenna length approaches a quarter wavelength. This section examines differences between the 4cm and 10cm dipole, and discusses the effects of the cavity on the current distribution of the antenna.

The field distribution for the 10cm dipole over the 200-700MHz range is very similar to the 4cm dipole. A noticeable difference can be seen Figure 4.15 in which the relative strength of the Ey fields is greater for the 10cm dipole. Because the plots are normalized, it's difficult to compare them. What can be stated though is that for the 10cm dipole the Ey field strength at lower frequencies is stronger with respect to its maximum than the same frequencies for the 4cm dipole. The null discussed earlier is also shown in Figure 4.15, but occurs at a different frequency for the 10cm dipole. The null radius is affected by the size of the antenna in addition to frequency. Since the near field distribution is directly related to the size of the antenna, and the null is formed by destructive interference from reflected fields and the radiated near fields from the dipole, the null is therefore related to the size of the antenna. Lastly, there is also a slight shift in the resonance frequency; for the 10cm dipole it occurs at 632MHz. This same effect was seen in [8-10] and is due to the volume of the dipole in the cage. This effect is akin to that of a dipole in free space having a slightly lower resonance than 0.5λ due to its radius [21].

The biggest difference between the two dipoles is seen by examining the input impedance and current distribution on the antenna. Figure 4.16 and Figure 4.17 are comparisons of the reactive and real impedances. There is little change in the real impedance between the two dipoles other than a small increase. The impedance magnitude for the 10cm dipole however is much greater than the 4cm. The reactive resistance for the 10cm dipole

crosses zero and behaves asymptotically as it approaches resonance, exhibiting attributes similar to a full wave dipole in free space. Explanation for this difference can be found by examining the current distribution on the two antennas.

Investigation of the current on the 4cm and 10cm antennas, revealed two completely different distributions. Figure 4.18 shows the difference between the current on the two dipoles at cavity resonance. The 10cm dipole has a current distribution for a full wave dipole in free space, while the 4cm antenna still resembles that of an electrically small dipole. Even though resonance of the 10cm dipole is 3GHz, the cavity resonance is altering the current distribution and forcing the antenna to behave like a full wave dipole at a much lower frequency. This same effect was seen in [8] for a high Q cavity. However, in [8] the dipole had to be a quarter wavelength at cavity resonance, a slightly shorter λ/5 antenna did not exhibit a full wave current distribution. Simulations with NEC for the animal cage showed a full wave current distribution was attainable down to a 7.5cm dipole, or about 0.16λ at cavity resonance. The current distribution on antennas smaller than this appeared similar to that of an electrically small dipole. Since the cavity is altering the current on the antenna, this results in a change of the input impedance. By forcing a full wave current distribution on the 10cm dipole at resonance, the input impedance increases to resemble a full wave dipole in free space. The 4cm dipole was not forced to a full wave current distribution; consequently the changes in input impedance were minimal compared to the 10cm dipole.

In review, the field distribution and excitation of the TE^{z}_{101} mode appears unaffected by the size of the dipole. The null around the antenna, is dependent on the frequency and size of the dipole. It was also discovered that the cavity forces a full wave current distribution on a dipole antenna larger than 0.16λ. This suggests that small, inefficient antennas in free space can couple efficiently to the wire-mesh animal cage.

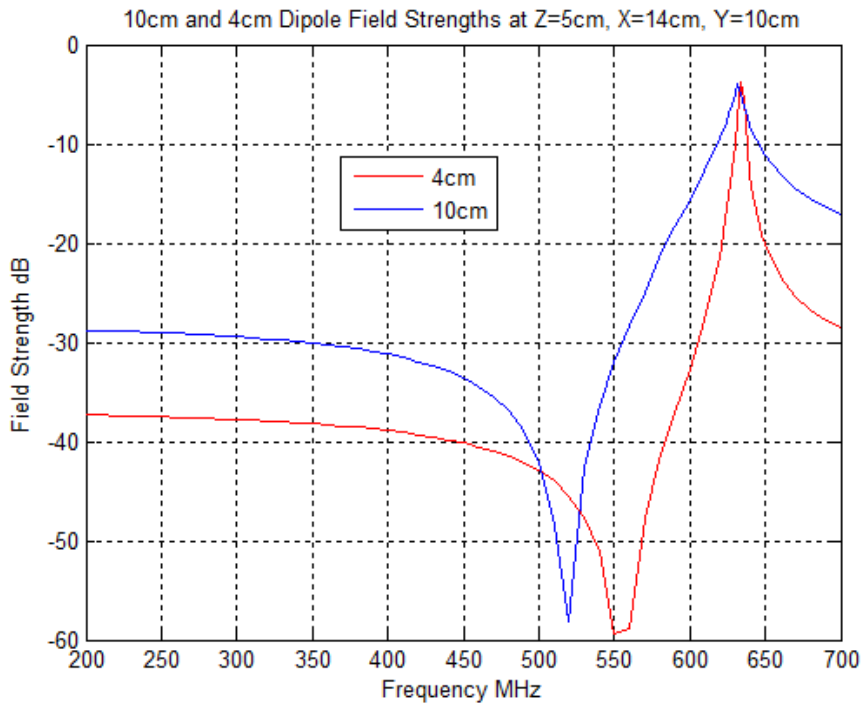

Figure 4.15: 10cm and 4cm Dipoles at X=5cm, Y=14cm, Z=10cm

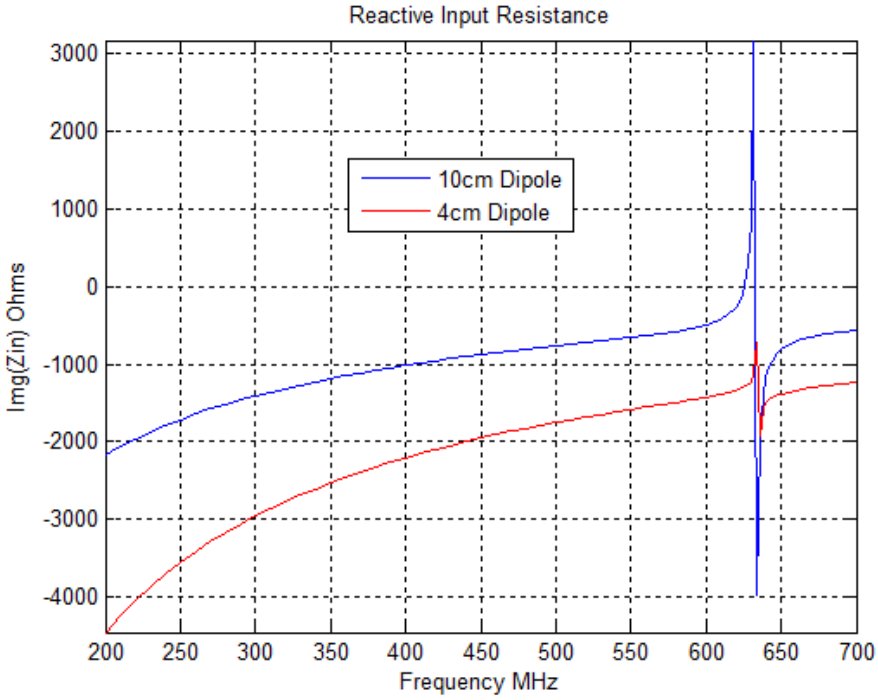

Figure 4.16: 10cm and 4cm Dipole Reactive Resistance

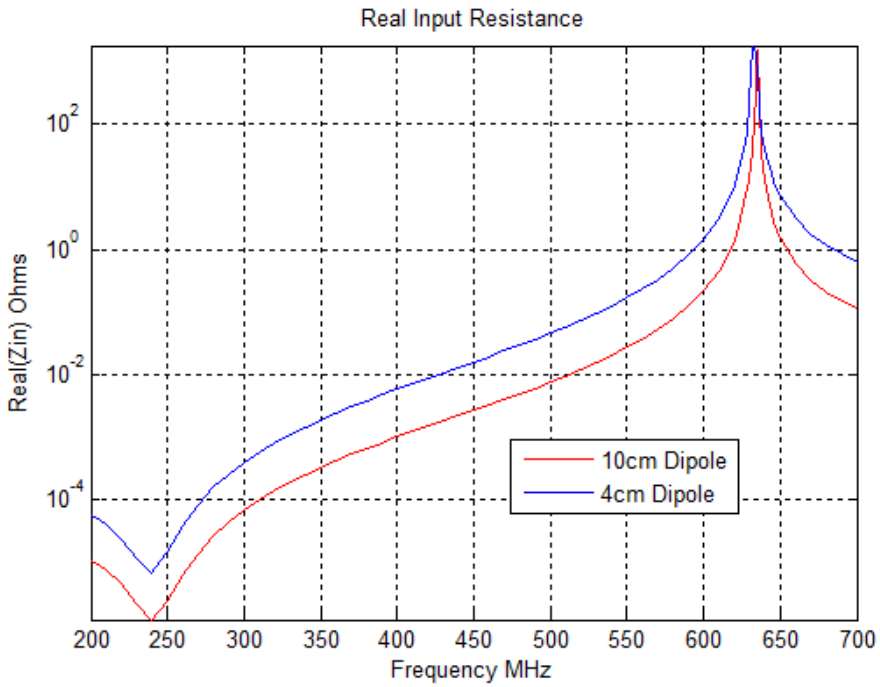

Figure 4.17: 10cm and 4cm Dipole Real Resistance

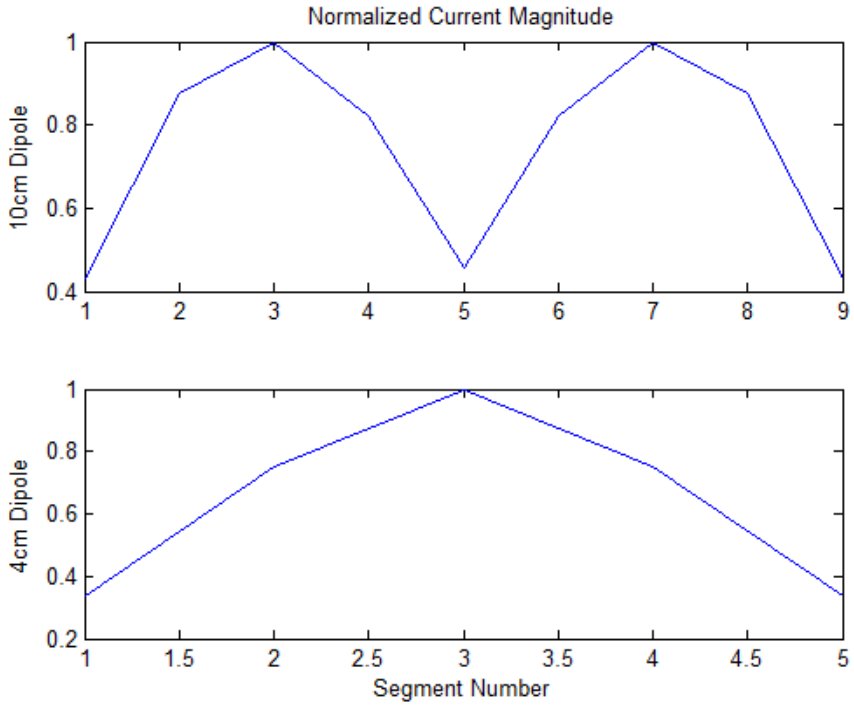

Figure 4.18: Normalized Input Current Magnitude

4.3 Effects of Antenna Position

Previously the dipole was only located at the center of the cage, in this section the position of the antenna is now varied. Moving the vertically orientated dipole to different locations within the animal cage affected the physical characteristics of the antenna as well as coupling to the TE_{101}^{z} mode. Dramatic differences were seen in data collected for antenna positions near the edge of the cage in comparison to previous data with the dipole at the center.

Positioning the dipole at locations near the cage walls resulted in weaker coupling to the mode. Figure 4.19 and Figure 4.20 are contour plots of the 4cm dipole located near the side and in the corner of the cage at 433 MHz. As can be seen, the null due to the near field characteristics of the antenna is still present and moves with the dipole. The null also does not extend outside the cage. If the frequency is increased to resonance at 634 MHz, the null disappears and the TE_{101}^{z} mode is excited - Figure 4.21. Looking at Figure 4.22, this shows the trend lines for three different dipole locations. It shows that the strength of the coupled fields within the cage is much less when the dipole is positioned where the TE_{101}^{z} mode is weaker. There is no evidence to suggest that antenna location affects the resonant frequency of the cage.

In a true cavity, the $\vec{E}$ fields would be evanescent below cutoff and all the energy would be reflected back within the cage at the walls. However, in this case much of the energy is passing through the mesh and propagating outside. This can be explained with transmission line theory. The cavity wall should act as a short circuit, reflecting all the energy back (S_{11} would be one). However the mesh has real and imaginary impedance, creating non-zero impedance. This is responsible for leakage out of the cage, some of the energy is reflected at the wall, some is dissipated, and the remainder is transmitted. This in essence allows the $\vec{E}$ field to extend

beyond the walls instead of completely going to zero, thus permitting longer wavelengths and a lower resonant frequency. The $\vec{E}$ fields reflected back within the cage undergo a phase change, which results in the null previously discussed. The proximity of the dipole to the edge of the cage does not seem to affect the amount of leakage at cage resonance, however below resonance there is a noticeable increase when the antenna is near a wall.

Position also directly affects the antenna characteristics; this is seen by examining the input impedances as well as the current distribution. Figure 4.23 and Figure 4.24 are plots of the real and reactive impedances of a 4cm dipole as the antenna is moved to three different locations. Moving the dipole away from the center resulted in decreasing impedance. Recalling the sharp increase in reactive input impedance for the 4cm dipole at the center of the cage, this effect has nearly disappeared with the antenna now near the edge of the cage. Whereas previously the dipole took on full wave current distribution characteristics at resonance, it now seems to retain its free space attributes as it moves away from the center. Figure 4.25 shows that at cage resonance as a 10cm dipole moves towards the edge, the current distribution shifts away from that of a full wave distribution back to an electrically small antenna current distribution. Since the dipole is moving to a location where the $\vec{E}$ field is weaker due to the distribution of the TE_{101}^{z} mode, the effects of the modal $\vec{E}$ field on the dipole are less. Consequently, the induced currents on the antenna are not forming a full wave dipole distribution and the impedance does not increase as much.

In conclusion, several statements can be made about a dipole antenna inside the wire mesh animal cage. First, the cage supports the TE_{101}^{z} mode but at a lower frequency than a similar enclosure with solid walls. This is due to the inability of the mesh to act as a solid conductor and force the $\vec{E}$ field to zero at the walls. Depending on the size of the antenna, the resonance of the cage is around 634 MHz. A second statement can be made in regards to the

null. The result of destructive interference from reflected fields and radiated fields, the null is dependent on the frequency and size of the antenna. It is centered on the middle of the dipole, has a sphere like shape and moves if the dipole is placed at a different location. Third, the current and input impedances of the dipole are altered by the cavity at resonance. Both real and reactive impedances sharply increase. If the dipole is 0.16λ or larger, a full wave current distribution forms on the dipole. This effect is a result of the reflected $\vec{E}$ fields interacting with the antenna. Fourth, and lastly, the position of the antenna directly affects coupling to the mode and the impedance and current characteristics. As the dipole moves away from the center of the cage, the increase in impedance is much less and the current distribution shifts back towards that of an electrically small antenna.

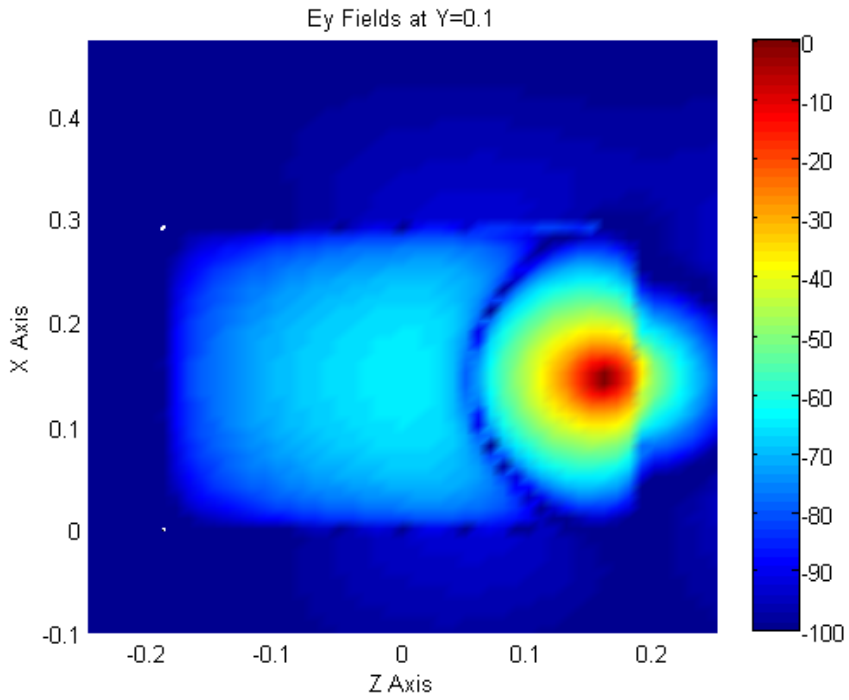

Figure 4.19: Ey Field Strength for Side Located Dipole at 433 MHz, dB

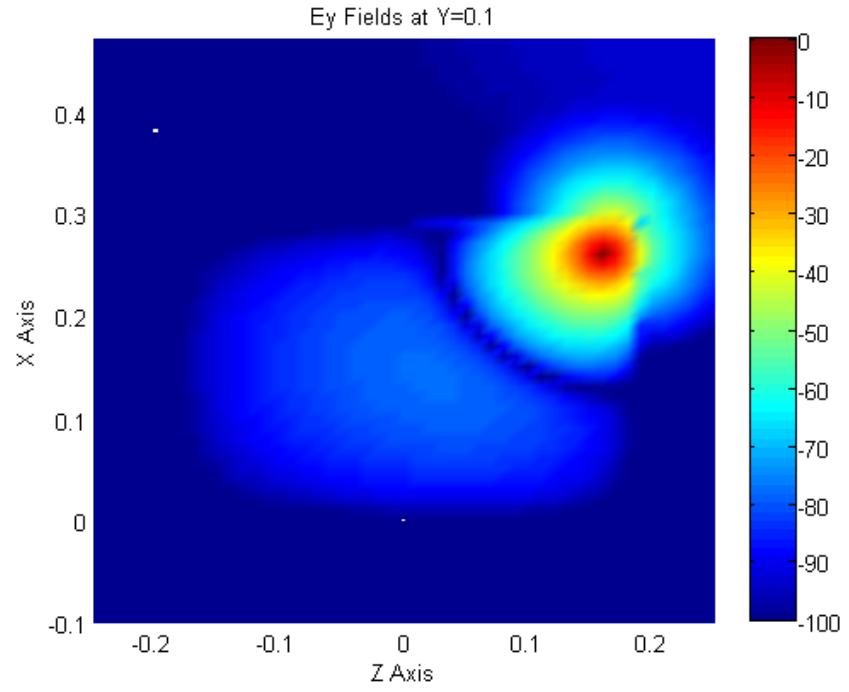

Figure 4.20: Ey Field Strength for Corner Located Dipole at 433 MHz, dB

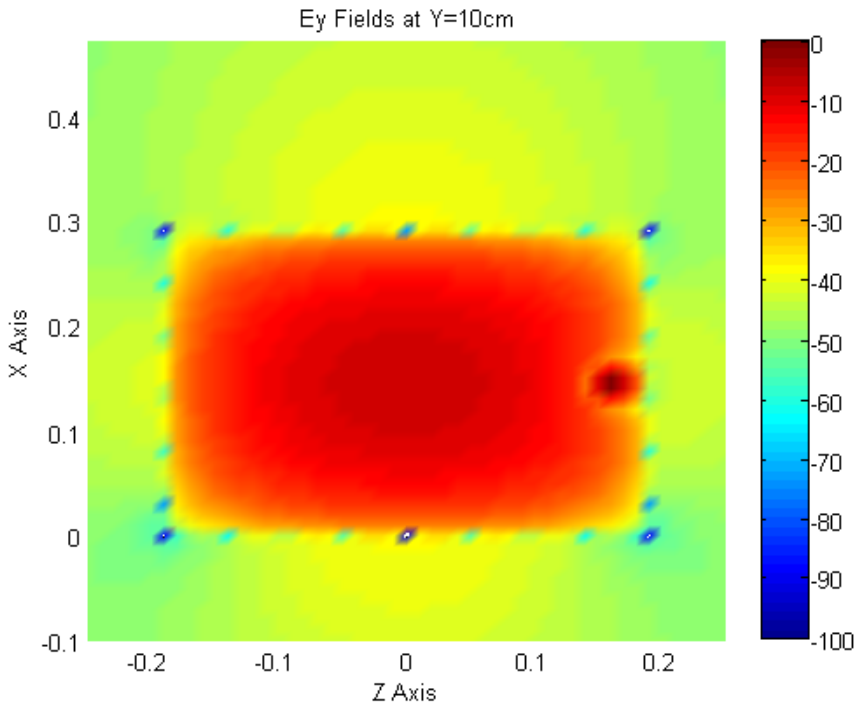

Figure 4.21: Ey Field Strength for 4cm Side Located Dipole at 634 MHz, dB

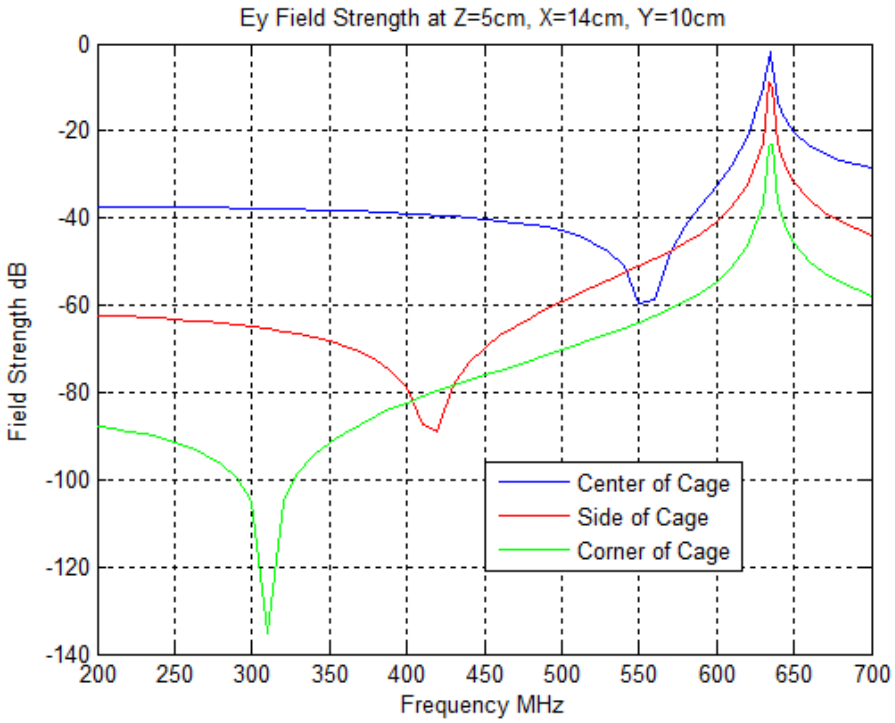

Figure 4.22: 4cm Dipole Ey Field Strength due to Changing Dipole Positions

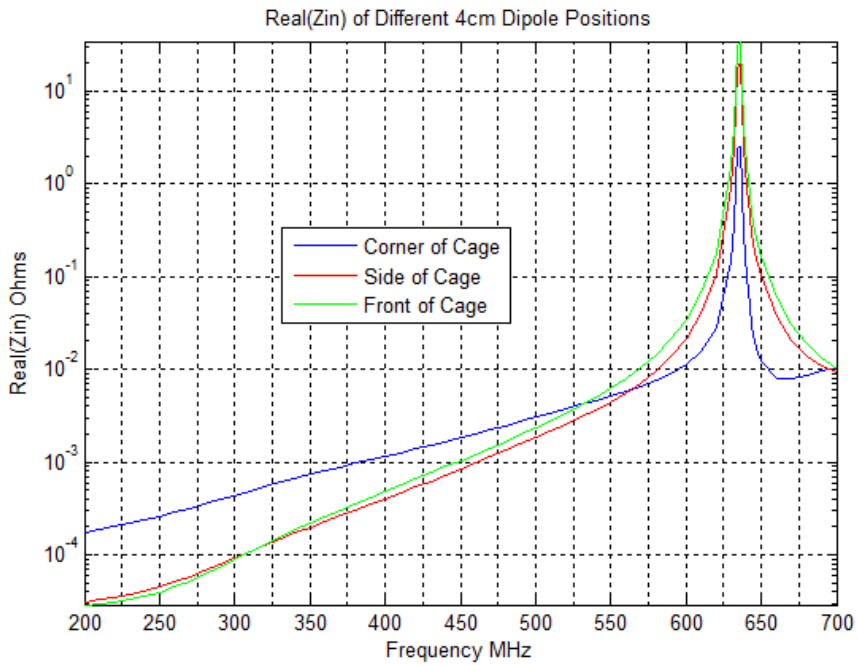

Figure 4.23: 4cm Dipole Real(Zin) at Various Positions

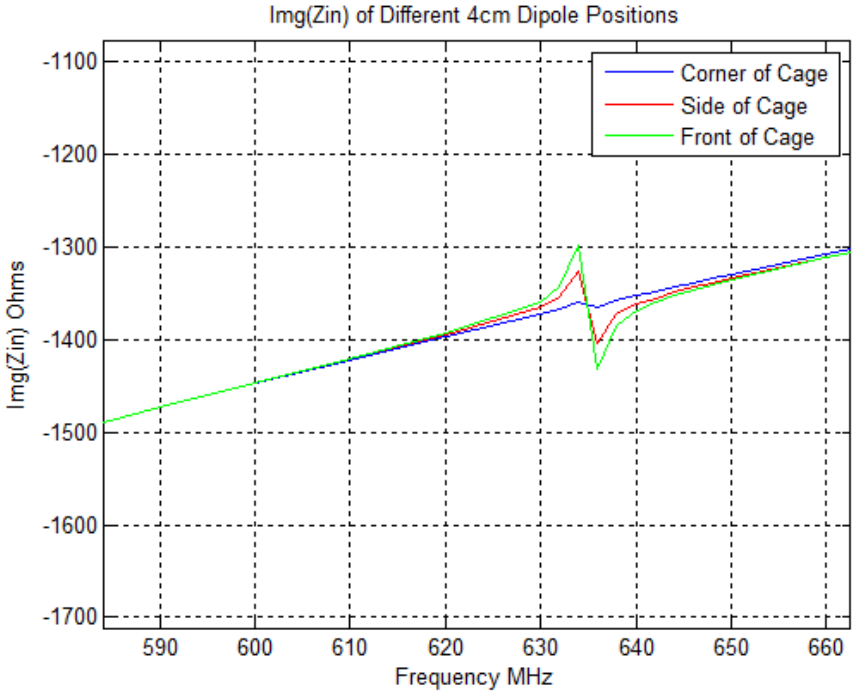

Figure 4.24: 4cm Dipole Img(Zin) at Various Positions

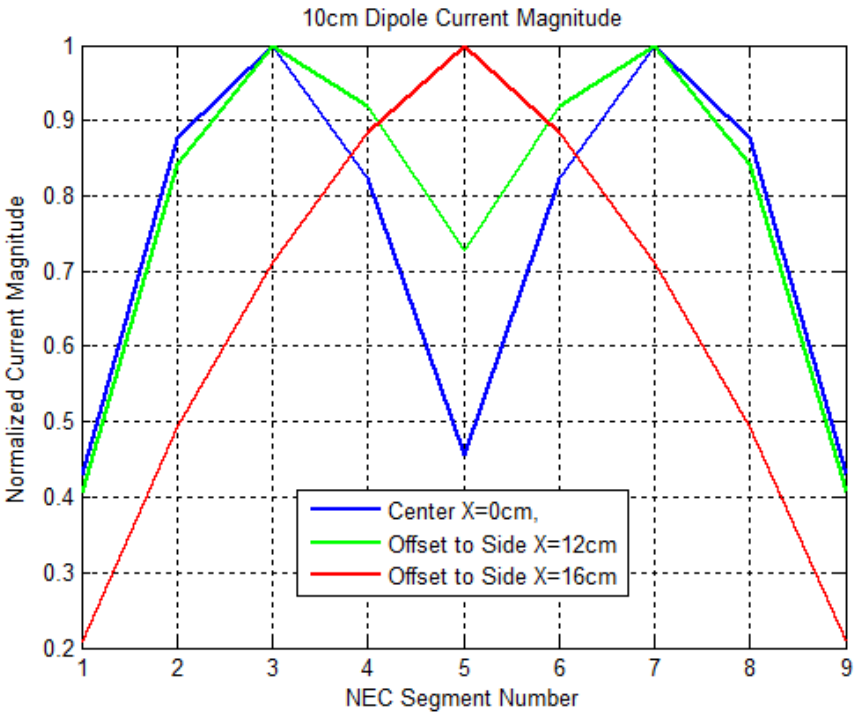

Figure 4.25: 10cm Dipole Current Magnitude as Antenna Moves Away From Center

5 Monopole Results

The monopole in this chapter is used to demonstrate the actual characteristics of the animal cage. This is accomplished through the use of NEC simulation data along with experimental results. The dipole from Chapter 4 has provided a basic understanding of the $\vec{E}$ field behavior and antenna parameters inside the cage. Chapter 5 will now demonstrate similarities between the monopole and dipole theoretical results, and experimentally draw conclusions about RF communication.

As with Chapter 4, a number of contour plots are shown in this chapter. Figure 5.1 demonstrates the plane for contour plots at Y=19cm, Figure 5.2 for plots at X=14cm.

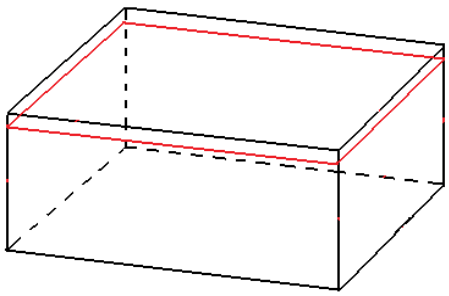

Figure 5.1: Plane of Contour Plots at Y=19cm

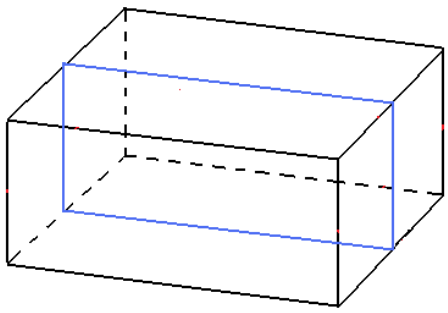

Figure 5.2: Plane of Contour Plots at X=14cm

5.1 Monopole Simulations

A large number of monopole simulations were done with NEC. Due to the many similarities with the dipole, similar results and effects were expected. As will be shown in this section, this was indeed the case. A brief summary of NEC monopole simulation results will be given in this section and related to effects seen with the dipole.

From the dipole results, it is clear that the TE^z_{101} mode can exist within the cage. It is therefore expected that the monopole will also excite the fields accordingly. This is the case, and the resulting field configuration seen in NEC is very similar to the dipole. Figure 5.3 is a contour plot cut through the center of the cage at a height of Y=19cm at 433 MHz, Figure 5.4 is cut through vertically at X=14cm. Only these two contour plots are shown to eliminate redundancy and highlight the location of the null. The monopole is located at the top of the cage, using the wire mesh wall as a ground plane. The null is centered on the feed point of the monopole (for NEC this is the segment where the excitation source is located). Beginning at 200 MHz, the null is at its largest and begins to converge on the feed point of the monopole as frequency increases – just like the dipole. At the lowest frequency of 200 MHz, the edge of the null is at the cage walls and extends about 8cm down from the top of the cage. Since the monopole is using the cage wall as a ground plane, the null is shaped like a half sphere that is stretched horizontally.

As with the dipole, the monopole simulations also exhibit large changes in input impedance as the frequency approaches cavity resonance. Recall from Chapter 4 that the impedance increase is due to the current distribution forced on the antenna from the cavity. Figure 5.5 is a plot of the reactive impedance for two different sized monopoles. As can be seen, the reactive impedance behaves just like the dipole (real input impedance also behaves similar to the dipole but is not shown). Figure 5.6 is a plot showing the current distribution of an

8cm monopole and 2cm monopole. The current resembles that of a half wave monopole in free space for longer antennas. As the antenna length is reduced, the current distribution shifts back towards that of an electrically small monopole. This same effect was seen with the dipole in Chapter 4. The monopole continues to exhibit half wave current distribution characteristics until its length is less than 0.085λ at cage resonance.

The monopole is very similar to the dipole when the characteristics of both antennas are compared in free space [21]. This section has briefly shown that when placed inside the animal cage, the monopole still acts very similar to the dipole. Both antennas excite the TE_{101}^{z} mode, and along with it a null that converges on the feed point of the antenna. The wire mesh animal cage also forces changes in the current distribution on both antennas at cavity resonance, provided that the antenna is longer than a certain length. This current distribution is also responsible for the large impedance increase. Lastly, the monopole experiences reduced effects from the cavity as it is moved away from the center of the cage towards the sides. The current distribution shifts back towards an electrically small antenna, input impedance decreases, and the overall level of the field strength inside the cage also decreases. As with the dipole, this is related to the field distribution set up by the TE_{101}^{z} mode.

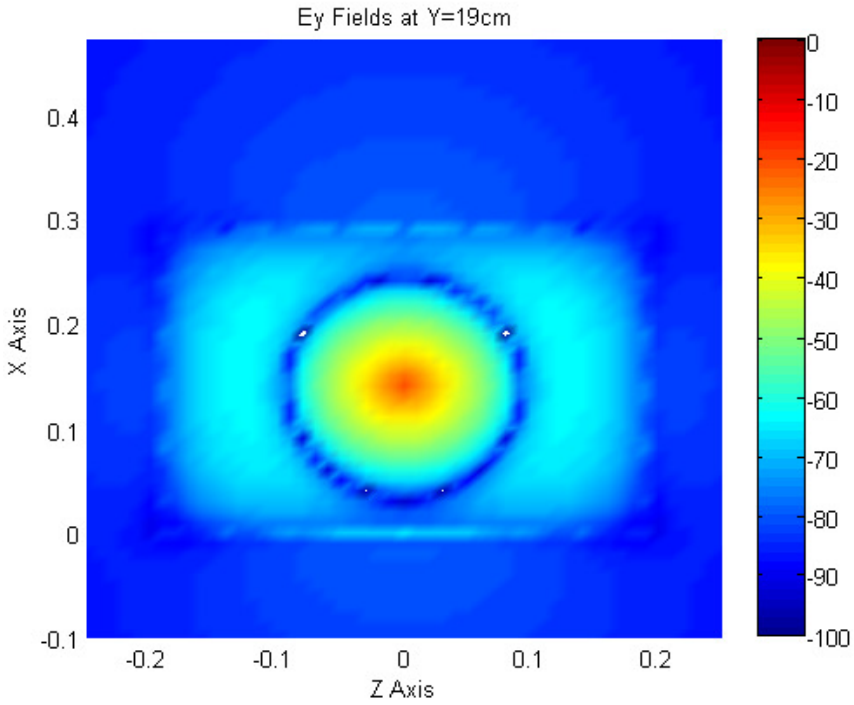

Figure 5.3: Contour Plot Ey Field Strength at Y=19cm, 433 MHz, dB

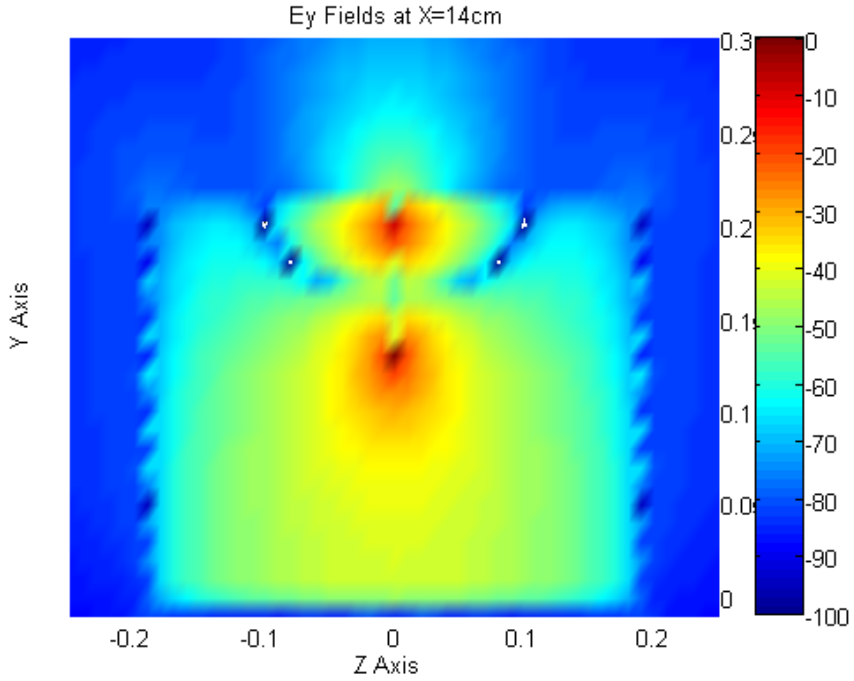

Figure 5.4: Contour Plot Ey Field Strength at X=14cm, 433 MHz, dB

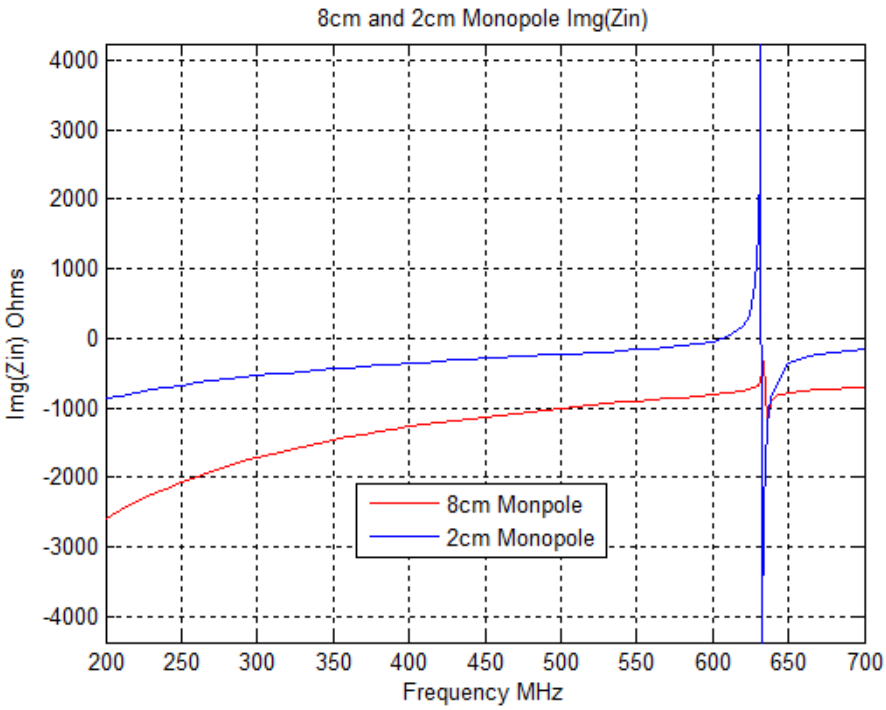

Figure 5.5: Zin(Img) for 8cm and 2cm Monopoles

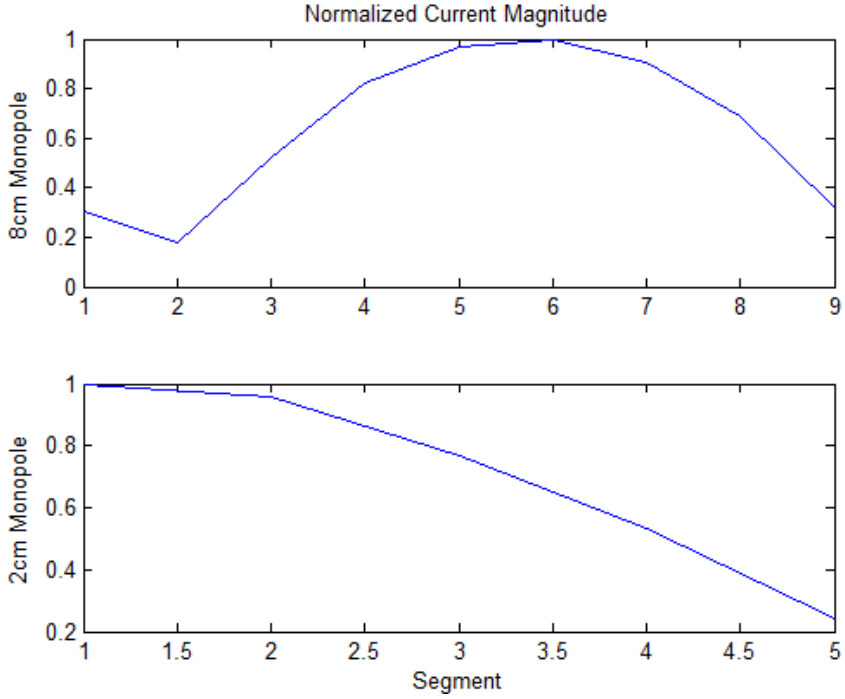

Figure 5.6: Current Distribution for 8cm and 2cm Monopoles at Resonance, 632MHz

5.2 Experimental Results

This section uses experimental results to demonstrate the effects seen in NEC simulations. With a vector network analyzer, S_{11} is used to analyze monopole behavior inside the animal cage, after which S_{21} is used to investigate the distribution of the mode and location of the null. This section concludes with a summary of ideal methods for RF communication between two monopole antennas inside the animal cage.

An 8cm monopole was placed at the center, side, and corner of the cage as diagramed by Figure 3.2. Figure 5.7 shows the results from the vector network analyzer measuring S_{11}, where S_{11} measures energy reflected back to the analyzer from the antenna. Smaller values of S_{11} indicate greater amounts of energy being radiated. Examination of Figure 5.7 shows a deep dip at 587 MHz when the monopole is positioned at the center of the top wall. This is the point at which the antenna is coupling the best and radiating the most energy. Since the input impedance is changing as frequency approaches resonance, the dip is the point at which the antenna-cavity system is matched closest to the 50-Ohm coaxial cable. Consequently, this is showing where the system is optimally coupled and that cage resonance is occurring at 587 MHz.

Examining Figure 5.7 again, it can be seen that when the monopole is located at the side or corners of the cage, S_{11} does not exhibit the deep dip that it does for the center. As the monopole moves away from the center of the cage, the effects of the mode decrease. The current distribution on the antenna is changing from a half wave monopole to an electrically small distribution. As a result the real and imaginary impedance of the antenna decreases. When the monopole is near the edges of the cage, input impedance does not change enough to match the coaxial cable at any frequency. There is a higher S_{11} and less energy radiated. The

monopole couples best to the cage when it is located at the center where the TE_{101}^{z} mode is strongest and can force a change in the current distribution.

S_{11} for a smaller monopole gives poor results in comparison to the 8cm monopole. Figure 5.8 displays S_{11} for a 4cm monopole at the center, side and corner. When the monopole is at the center of the cage, the smallest S_{11} drop is -1.5 dB. When the monopole was 8cm long, S_{11} dropped down to about -17dB. It was previously shown through NEC simulations that small antennas were affected less by the mode. Smaller antennas had reduced input impedance at cage resonance and produced weaker $\vec{E}$ fields. Figure 5.8 confirms this fact experimentally. The 4cm monopole is affected less by the mode, reducing coupling to the cage.

To examine RF communication within the cage, two 8cm monopole antennas were placed inside and S_{21} was used to measure transmission between them. Figure 5.9 shows the results of S_{21}, with the transmit antenna at the center of the cage and the receive set according to positions 2, 3, and 7 from Figure 3.2. Several important conclusions can be drawn from this figure. First, the frequency for maximum coupling between the two antennas changes slightly based on their position. Table 5-1 lists the antenna position and the frequency for maximum S_{21}. Similar to the effect seen for S_{11}, as the receive antenna moves away from the center of the cage coupling decreases. The receive antenna is not experiencing the impedance changing current effects near the edges of the cage due to the weaker $\vec{E}$ field.

Evaluating the strength of the fields in Figure 5.9 reveals that all three antenna positions have a 3-dB bandwidth between 30 - 40MHz, which implies a Q around 15 - 20. This is important because the S_{21} peak for all three positions is within 30MHz of each other. If an 8cm monopole is being used for communication, the designer can choose an operating frequency that will always be in the 3-dB bandwidth of the antenna system as long as one antenna is located at the top center of the cage. The second antenna can be located anywhere along the

top. This also works if the transmit and receive antennas are placed on the bottom of the cage. A low Q cage is very advantageous, as it allows for a generous 3-dB bandwidth.

S_{21} for the 4cm monopole shown in Figure 5.10 is much less than it was for the 8cm. Inspection of all three peaks shows that the field strength never grows above -20dB. With the 8cm monopole, up to -5dB was achieved. A smaller antenna simply does not couple to the mode as well as a larger one. Received power must be sacrificed if smaller antennas are going to be used.

The null, discussed throughout Chapter 4 and 5, is present and moves around as predicted in Figure 5.9 and Figure 5.10. However, the null is avoided in Figure 5.11 in which S_{21} for two 8cm monopoles is measured. Previous experimental data was taken with both the transmit and receive antennas at the same height. In Figure 5.11 the transmit antenna is located at the top of the cage while the receive is at the bottom. This is more realistic to a RF system that would monitor animals within the cage. However, the position of the antennas has an advantage. The null is centered on the feed point of the antenna and only extends a certain radius outward. With the antennas separated between top and bottom, the nulls of the two antennas never coincide. Consequently, there is no “bad” spot for communication inside the cage. As long as there is enough vertical distance between the two monopoles, the nulls will not prevent coupling.

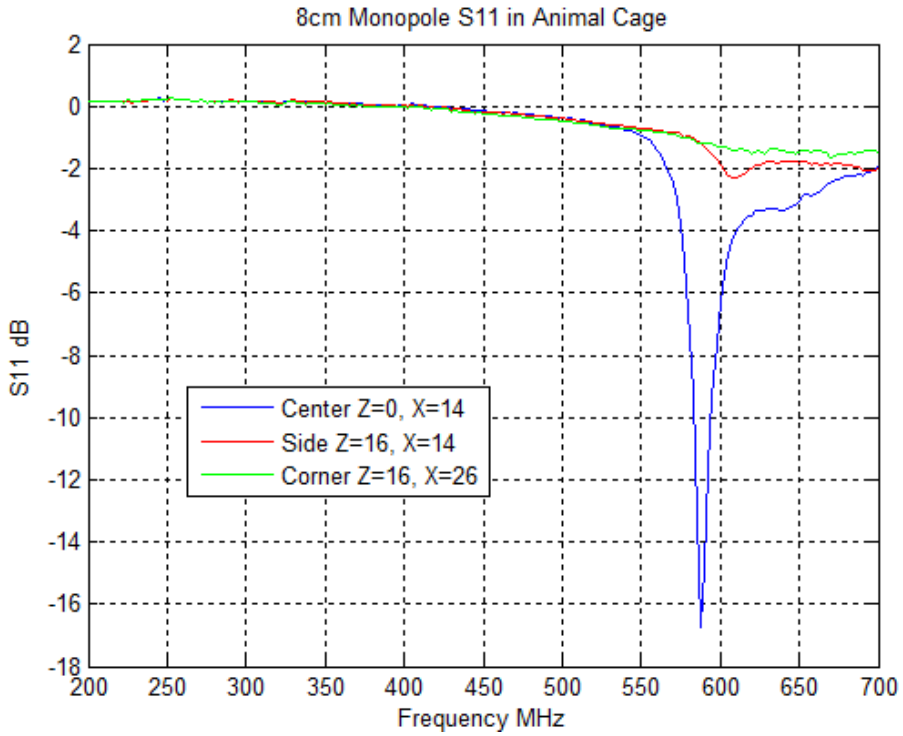

Figure 5.7: S11 for 8cm Monopole

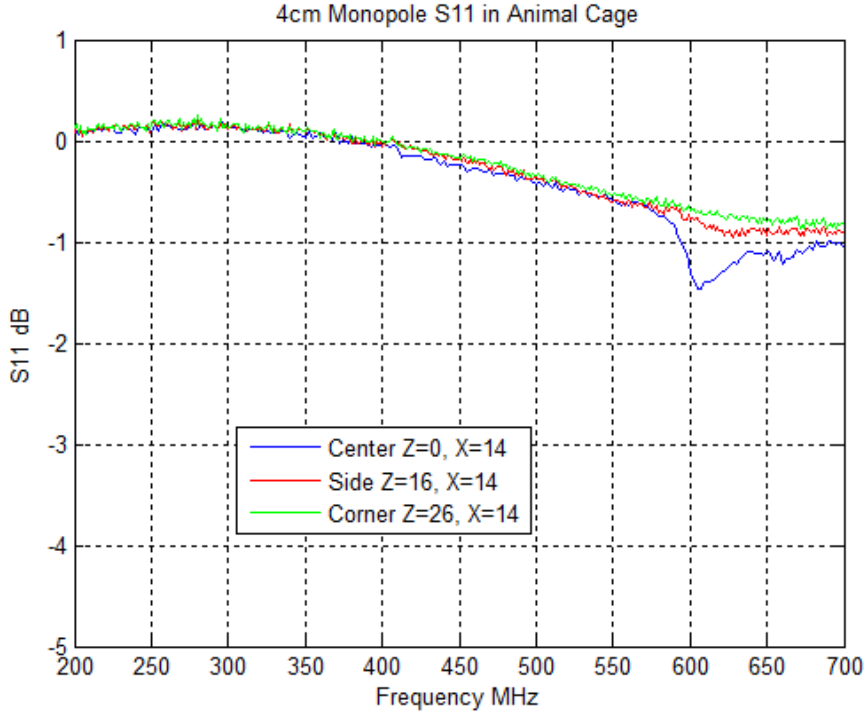

Figure 5.8: S11 for 4cm Monopole

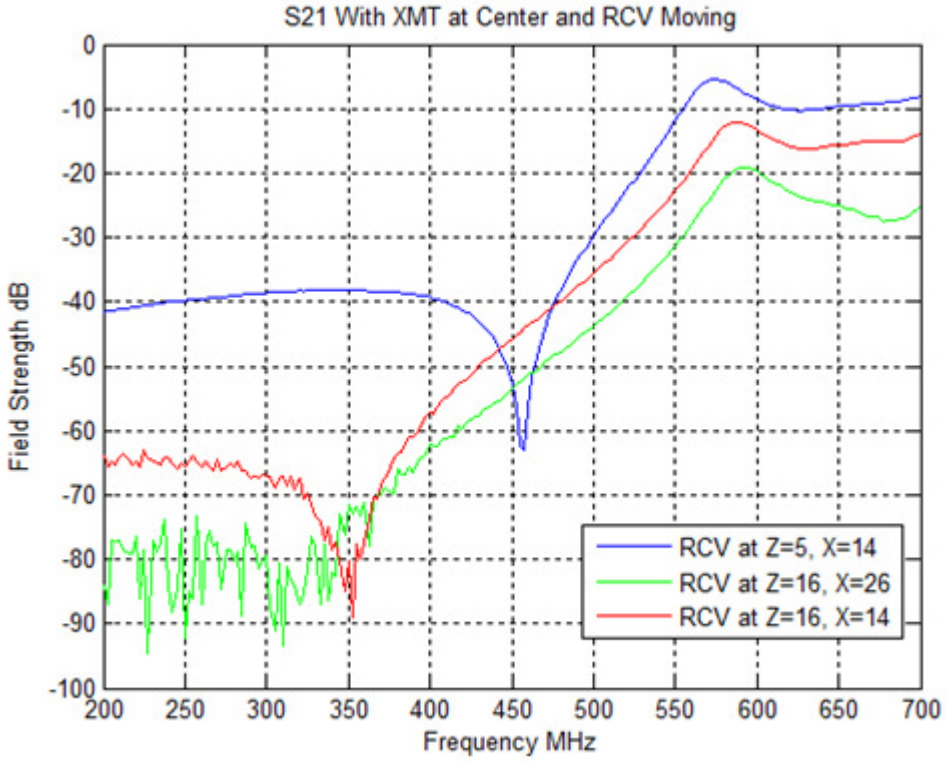

Figure 5.9: S21 for 8cm Monopole

Receive Antenna Location	Frequency of Max S_{21}	Max S_{21} dB	3-dB Range (MHz)
Z=5cm, X=14cm (offset from center)	572 MHz	-5.37	560-597
Z=16cm, X=14cm (side of cage)	587 MHz	-12.07	572-612
Z=16cm, X=26cm (corner of cage)	590 MHz	-19.12	580-610

Table 5-1: 8cm Monopole S21 Results

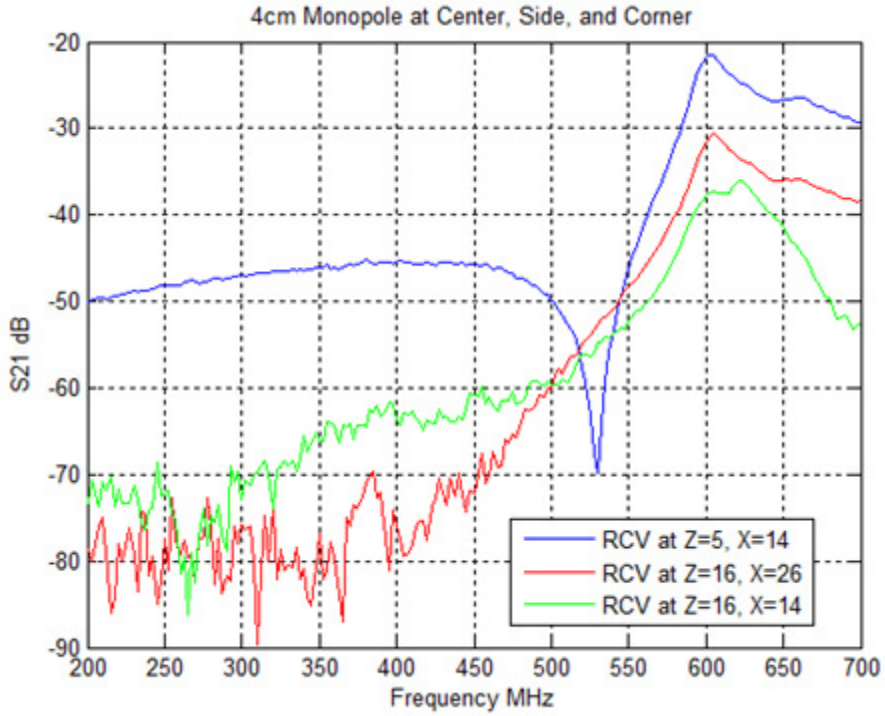

Figure 5.10: S21 for 4cm Monopole

Receive Antenna Location	Frequency of Max S_{21}	Max S_{21} dB	3-dB Range (MHz)
Z=5cm, X=14cm (offset from center)	602 MHz	-21.57	592-620
Z=16cm, X=14cm (side of cage)	605 MHz	-30.59	595-622
Z=16cm, X=26cm (corner of cage)	622 MHz	-36.12	595-637

Table 5-2: 4cm Monopole S21 Results

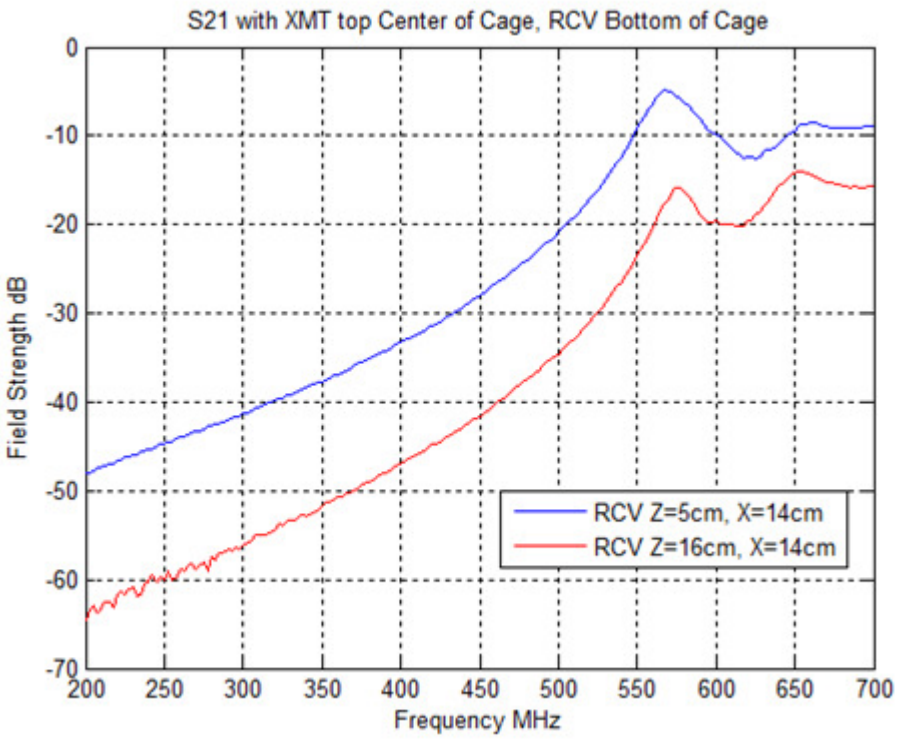

Figure 5.11: XMT on Top of Cage, RCV on Bottom

5.3 True Cavity Comparison

The purpose of the true cavity was to provide a comparison for the wire mesh animal cage (throughout this section "true cavity" will always refer to the solid PCB board cavity, and the wire mesh cavity will be referred to as the "wire mesh animal cage"). Monopole experiments inside the true cavity will demonstrate differences in antenna behavior between the two enclosures. The true cavity will induce similar effects on the antennas as the wire mesh animal cage. It will be shown that the low Q characteristics of the wire mesh animal cage are advantageous for RF communication.

The 8cm monopole behaves differently in the wire mesh animal cage than the true cavity. Figure 5.12 is a comparison of S_{21} in both enclosures with an 8cm transmit monopole at position 1 and an 8cm receive monopole at position 2 (positions according to Figure 3.2). Peak coupling for S_{21} inside the true cavity shifted up to 605 MHz, but is over 20dB less. Examination of S_{11} showed that the 8cm monopole was not coupling to the true cavity like it does for the wire mesh animal cage. Investigations in Chapter 5 showed that a half wave current distribution is being forced on the antenna inside the wire mesh animal cage at resonance even though the monopole is much less than a wavelength. A previous study [10] showed that inside a high Q cavity a dipole antenna must be at least $\lambda/4$ in length to experience the current altering effect. The 8cm monopole is not coupling well to the true cavity because it is not long enough to have a half wave current distribution forced on it. However, due to the low Q of the wire mesh animal cage the monopole does not need to be as long to experience the current altering effects.

When the monopoles are shortened to 4cm, the wire mesh animal cage still outperforms the true cavity. Figure 5.13 is a comparison of S_{21} with a 4cm transmit monopole at position 1 and a 4cm receive monopole at position 2 (positions according to Figure 3.2). The

two plots are relatively similar until resonance is approached. The peak $\vec{E}$ field for the true cavity occurs at a much higher frequency and spikes a little stronger than the wire mesh animal cage. The 4cm monopole is not coupling well to either enclosure. However, the overall level of field strength in the wire mesh animal cage seems to be much stronger than the true cavity. Because the monopole is coupling better to the wire mesh animal cage, it has an advantage over the true cavity. The low Q of the wire mesh animal cage allows for a greater range of frequencies to couple to the resonant mode and results in stronger fields.

The low Q of the wire mesh animal cage has shown to be very advantageous in this section. In comparison to the true cavity, much smaller monopole antennas can be used in the wire mesh animal cage to couple to the first resonant mode. Even if the antenna is not coupling well, the field strength is still much greater inside the wire mesh animal cage. This creates a good environment for RF communication, allowing for a large range of operating frequencies and a less sensitive receiver.

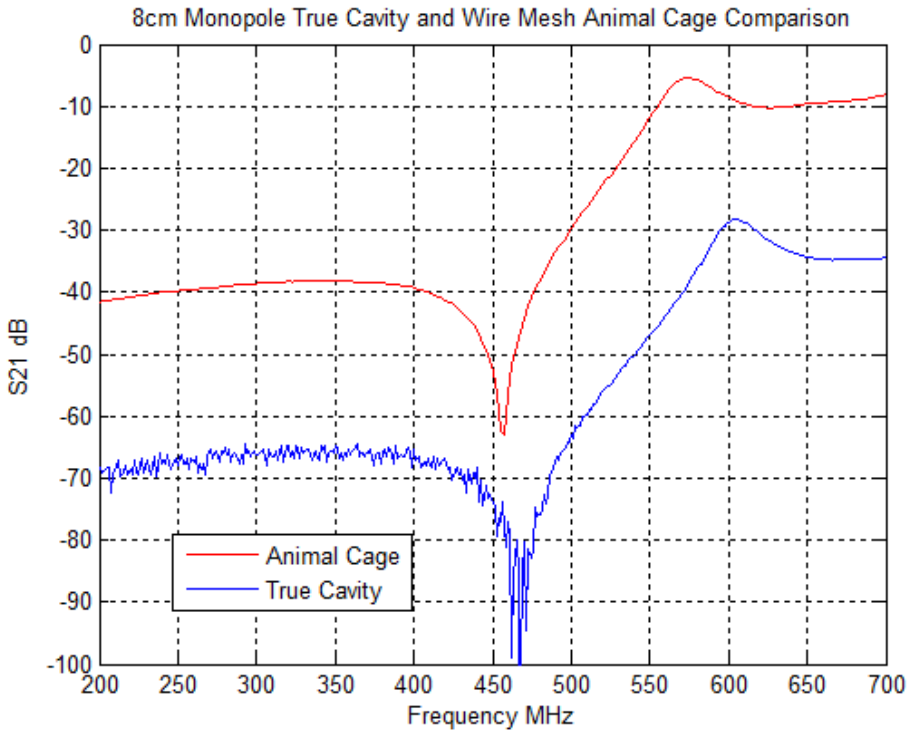

Figure 5.12: 8cm Monopole Cavity Comparison - XMT at Center, RCV Offset

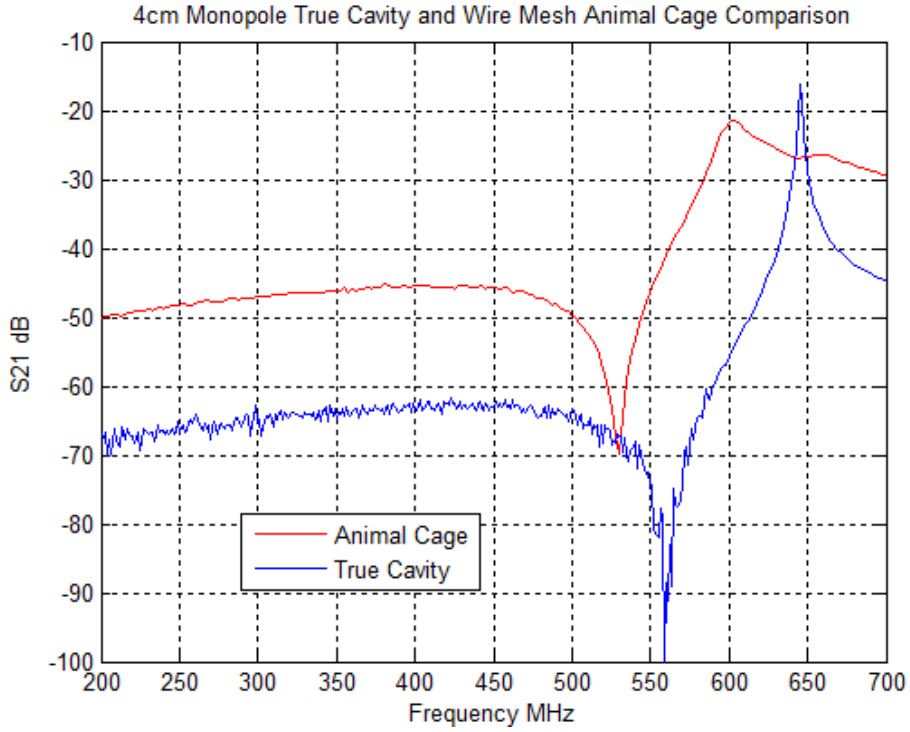

Figure 5.13: 4cm Monopole Cavity Comparison - XMT at Center, RCV Offset

5.4 Monopole RF Summary

The monopole results in this chapter have demonstrated that antenna coupling within a low Q cavity for RF communication is possible. The antenna positions must be judiciously chosen, such that nulls from the monopoles are avoided. Optimal positioning is one monopole at the top center of the cage pointing downward and another on the bottom pointing up. Since the antennas are reciprocal devices, there is no restriction on which antenna must transmit or receive. Additionally, it was shown that placing one antenna at the center of the cage allows the second to be anywhere within the cage at the same height and remain close to the 3-dB bandwidth. Lastly, the size of the antenna greatly affects coupling to the cage. Small monopoles will operate effectively but at the cost of received power.

Most likely a small antenna would be used if placed on an animal under observation. Placing a monopole or dipole on a rat or other small animal would be difficult but possible. The ability for effective RF communication relies heavily on coupling to the resonant mode. To achieve this, the antennas must be orientated vertically to excite the TE^{z}_{101}mode.

6 Loop Antenna

A loop antenna was evaluated inside the wire mesh animal cage to determine how a magnetic antenna would behave. The TE_{101}^{z} mode sets up strong electric fields near the center of the cage, but close to the sides magnetic fields dominate. This chapter will present a combination of NEC and experimental results for the loop antenna, and conclude with a summary on its feasibility for use in RF communication.

6.1 Simulation Results

This section demonstrates the ability of the loop to excite the first resonant mode of the animal cage. The antenna is placed near the sides of the cage at several different locations as described by Figure 2.14 for maximum coupling to the magnetic fields in the TE_{101}^{z} mode. It will be shown that the loop does excite the first mode in a similar manner to the dipole, but without the large null surrounding the antenna.

The contour plots in Figure 6.1, Figure 6.2, and Figure 6.3 demonstrate the ability of the loop to excite the first mode within the animal cage. Unlike the monopole and dipole, there is no null that converges from the edges of the cage to the loop. This is a result of the loop being a fundamentally different antenna. The null was previously caused by destructive interference related to the near field of the dipole/monopole. Figure 6.4 is a trend line of the Ey field strength inside the cage just offset from the center. This graph again shows the absence of any null, and that the $\vec{E}$ fields grow slowly but increase rapidly near resonance.

The input impedance and current distribution of the loop are relatively unaffected by the cage. Figure 6.5 demonstrates the slight change in reactive impedance at resonance. It is very similar to the changes seen for the small 4cm dipole and 2cm monopole, suggesting that the loop is not being affected very much by the cage. Further investigation into NEC results

showed that the current on the loop was not being forced to a full wave current distribution at cage resonance. The loop was very resistant to any effects from the cage seen earlier in Chapters 4 and 5.

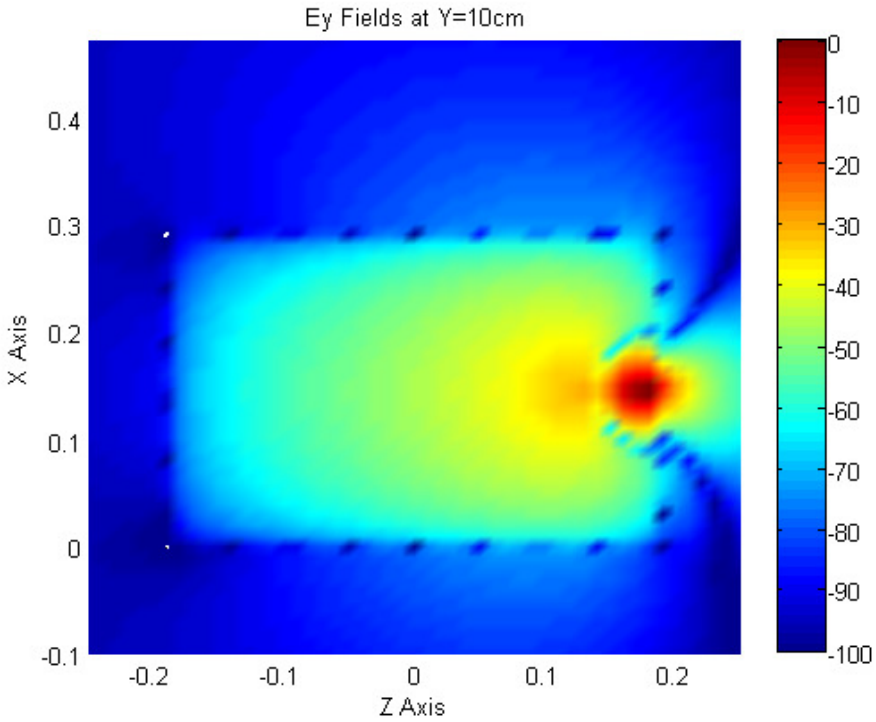

Figure 6.1: 3cm Loop Located at Side of Cage, 200 MHz, dB

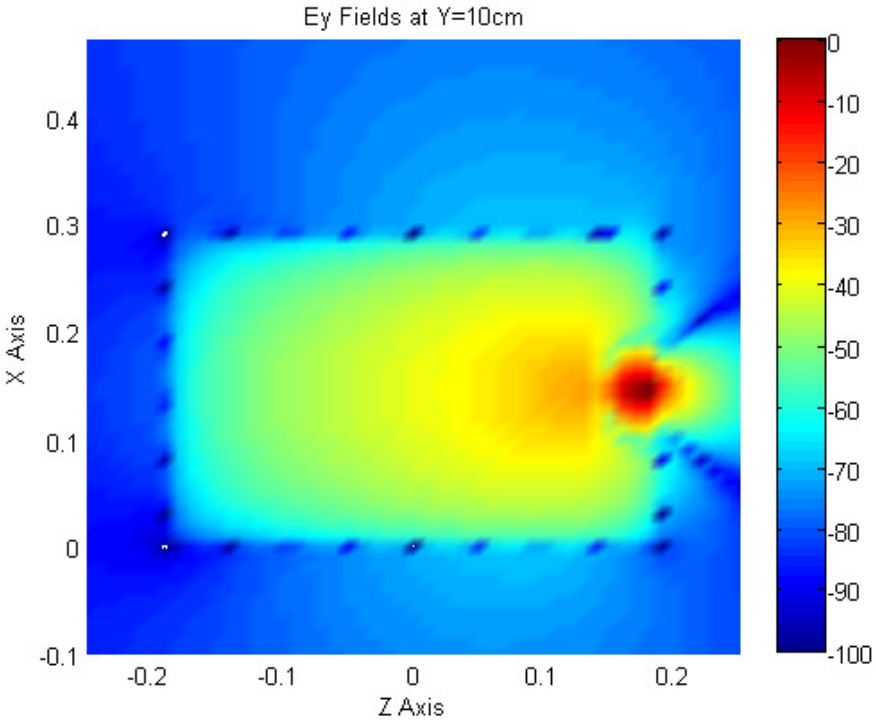

Figure 6.2: 3cm Loop Located at Side of Cage, 433 MHz, dB

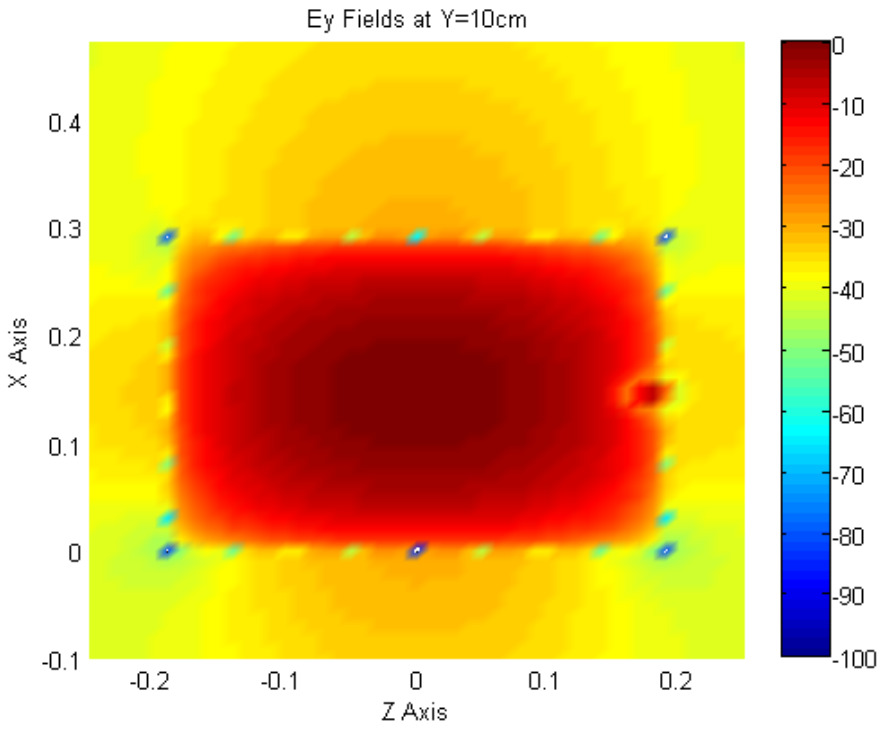

Figure 6.3: 3cm Loop Located at Side of Cage, 634 MHz, dB

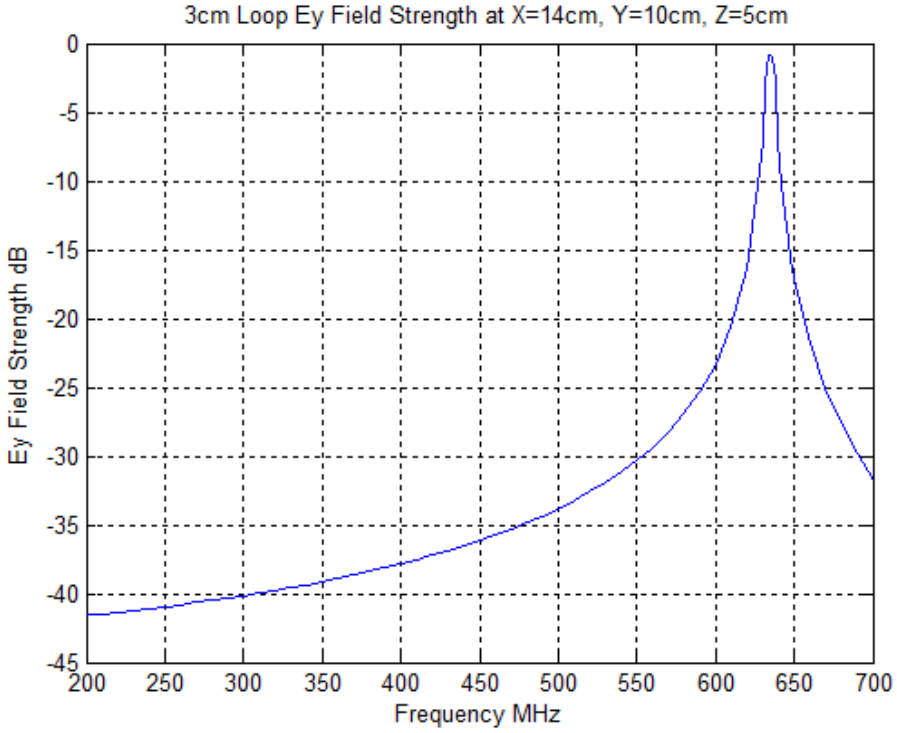

Figure 6.4: 3cm and 6cm Loop Ey Field Strength Trend

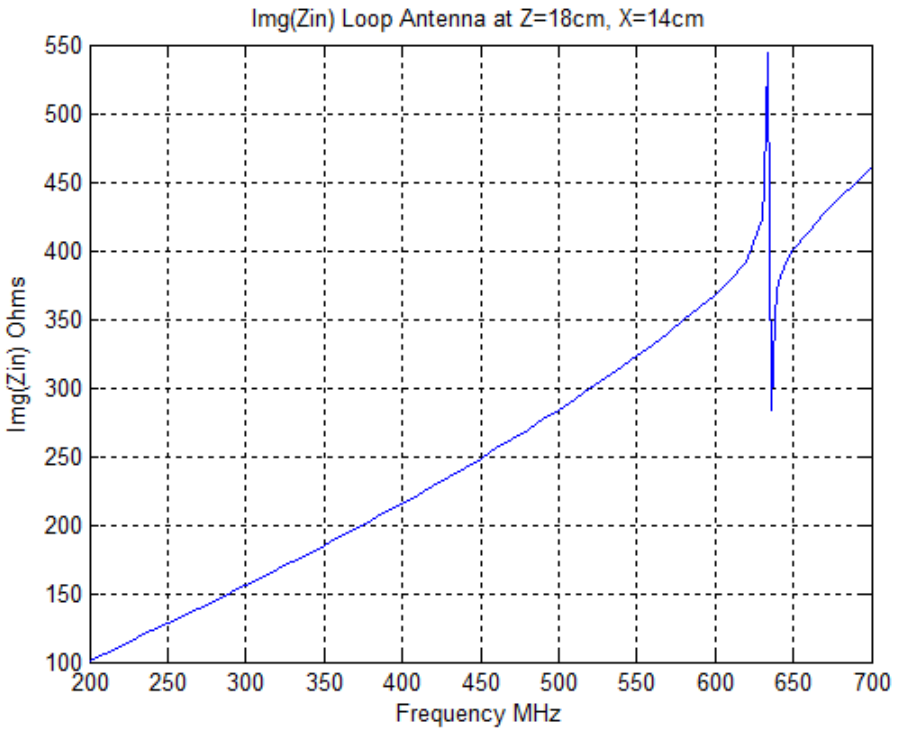

Figure 6.5: Img(Zin) of Loop at Side of Cage

6.2 Experimental Results

The loop antenna did not perform well experimentally in comparison to the monopole antenna. The loop was positioned for maximum coupling to the $\vec{H}$-fields near the sides of the cage pointing in, with its cross section in the vertical Ey plane (see Section 2.3.2 Antenna Location and Orientations). This section will illustrate that the loop is not an effective antenna for coupling to the TE_{101}^{z} mode for RF communication.

Loop to loop coupling inside the wire mesh animal cage did not produce good results. Figure 6.6 , Figure 6.7, and Figure 6.8 display S_{21} results for three different transmit and receive positions (Table 6-1 describes the loop locations for each figure). Unlike the monopole, there is no clear peak to indicate maximum coupling. As the frequency approaches resonance, the received power rises up out of the noise floor and steadily increases. Previous monopole experiments showed maximum coupling between the frequency range of 580 and 600 MHz and up to -5dB received. The loop at in this range is -50dB or lower. Moving the loop away from the side of the cage towards the center further decreased coupling.

Loop to monopole coupling produced better results than loop to loop. In Figure 6.9 the loop is located at the side of the cage (position 1 in Figure 3.3) and the monopole is located at the center and side (positions 1 and 3 in Figure 3.2). Unlike the loop to loop experiments, there is a clear peak of maximum coupling. In fact, there are two peaks. The first peak is when the monopole couples best to the cage, and the second peak is when the loop is coupling the best. The first peak decreases when the monopole is moved from the center of the cage to the side because it does not couple as well near the wall. The second peak has not changed because the loop did not move. However, moving the monopole has caused the null to appear. Previously, the null did not coincide with the loop, but with both antennas in close proximity it does.

Investigating S_{11} of the loop showed very little coupling to the cage. Shown in Figure 6.10, it appears that the animal cage has minimal effect on the antenna characteristics of the loop. However, as demonstrated by Figure 6.9, the loop does excite the TE^z_{101} mode. While the monopole couples to the cage very well, it is also heavily affected by it. The loop is more resistant to the effects of being inside the cage, but as a result it does not couple as well. In order for the loop to be effective, it must be located near the wall of the cage where the magnetic field is strongest. Moving it away from the side quickly reduces the little coupling it has.

Larger loop sizes were not investigated for several reasons. First, the loop had a limited range of positions in which it could effectively couple to the mode. The loop had to be placed very close to the side of the cage and with the cross section perpendicular to the wall. Tilting the loop so that it was not perpendicular immediately decreased coupling. Second, larger loops would protrude further into the cage. This would inhibit the movement of animals, and also move the center of the loop farther away from the side where coupling was best.

Description	Figure	Position Number Relative to Figure 3.3
Same Side Coupling	Figure 6.6	2 and 3
Opposite Side Coupling	Figure 6.7	1 and 4
Side to Front Coupling	Figure 6.8	1 and 5

Table 6-1: S21 Loop Antenna Locations

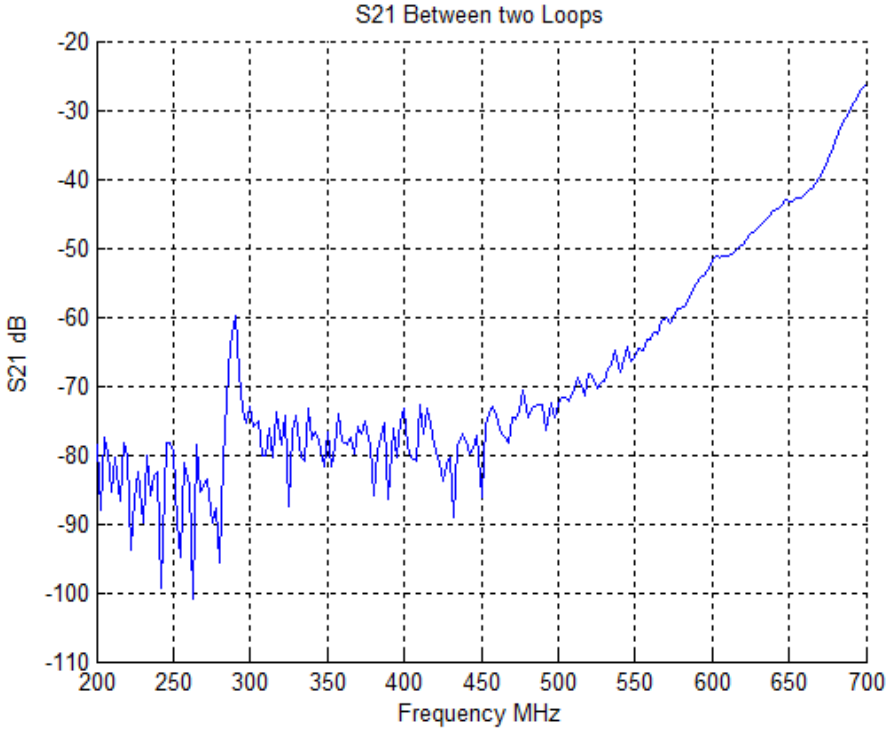

Figure 6.6: S21 Between two Loops 9cm Apart at Side of Cage

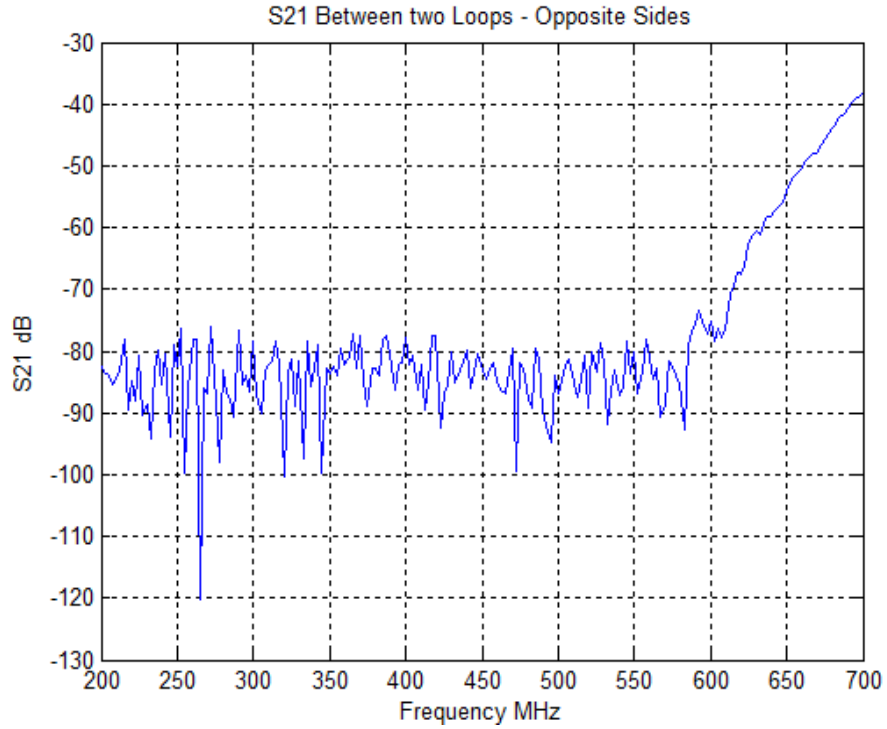

Figure 6.7: S21 Between two Loops on Opposite Sides of Cage

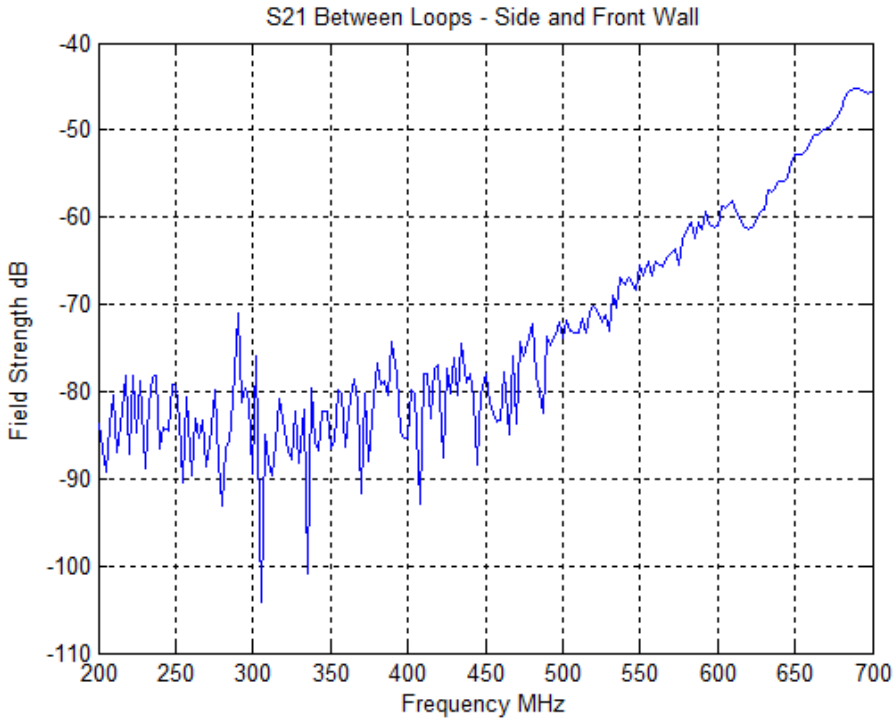

Figure 6.8: S21 Between two Loops, one at Side Wall and one at Front Wall

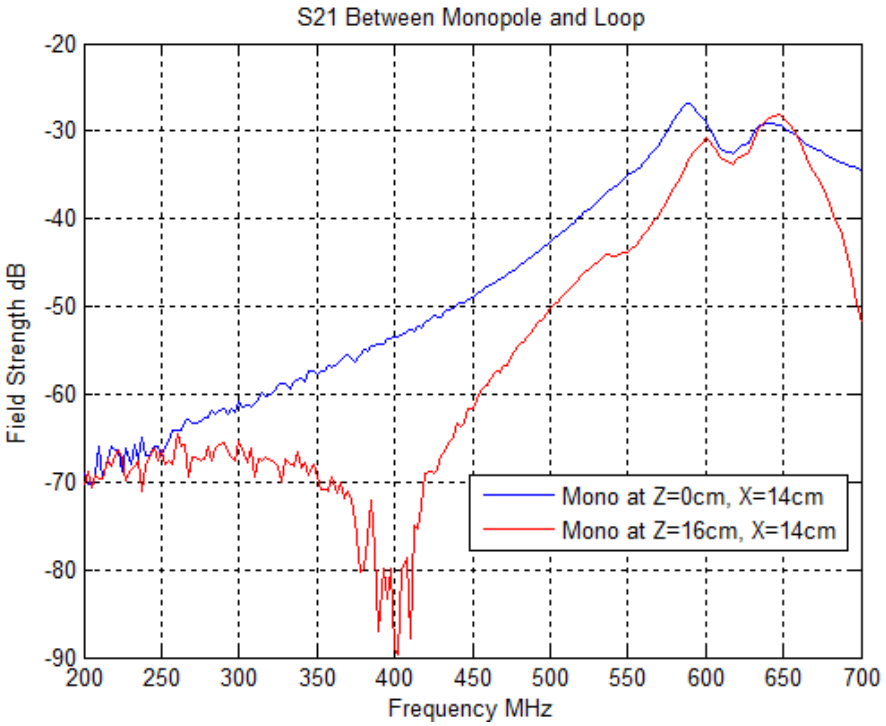

Figure 6.9: S21 Between 8cm Monopole and Loop

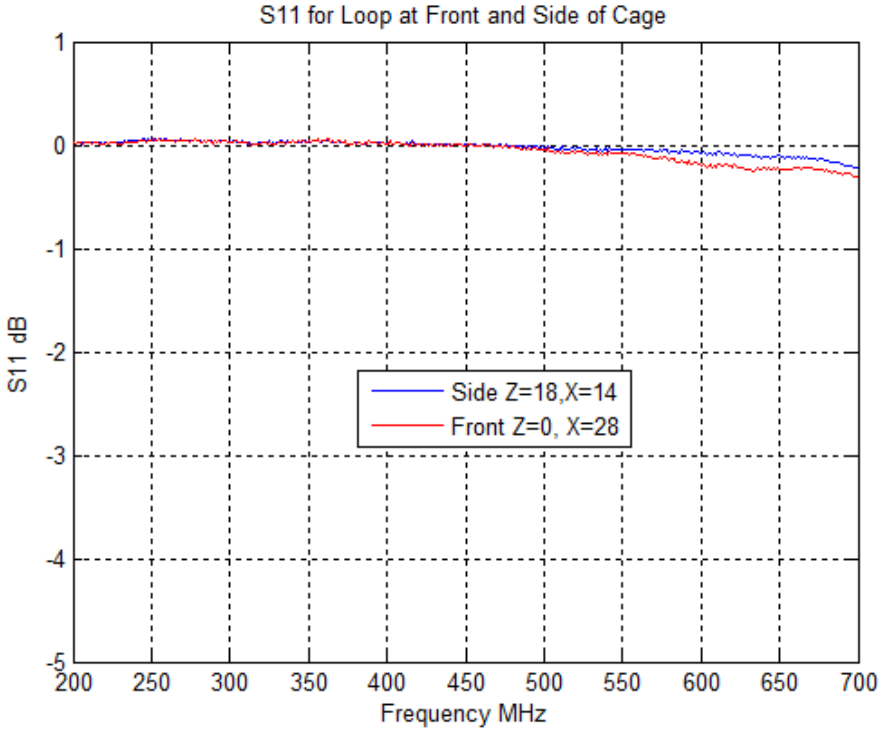

Figure 6.10: S11 of Loop

7 Discussion

7.1 Summary

This thesis has investigated the possibility of radio frequency (RF) communication by examining the field configuration within a wire-mesh animal cage from an internal radiator. A dipole, monopole, and loop, were considered as sources exciting the fields within a wire mesh animal cage. The development of various effects: modes, nulls, quality factor, current distribution, input impedance, and antenna location were investigated. The results of this thesis can now be summarized to provide a recommendation for RF communication.

NEC simulations demonstrated that the wire mesh animal cage supports the TE^z_{101} mode. The cage behaves like a low Q cavity. This allows for coupling to the TE^z_{101} mode well below resonance. Compared to a true cavity, the wire mesh cage provides a better environment for antenna communication. Chapter 5 showed that the monopole couples to the mode earlier in the wire mesh cage, and also achieved better reflection (S_{11}) and transmission (S_{21}) results.

However, the presence of the dipole and monopole inside the cage caused a boundary of destructive interference between the antenna near fields and developing mode. This destructive interference resulted in a null that began at the walls of the cage and converged on the feed point of the dipole and monopole.

The current distribution on the dipole and monopole antennas was dramatically affected by the presence of the cage. The $\vec{E}$ fields at cage resonance forced a full wave current distribution on the dipole and a half wave on the monopole, resulting in a large increase of input impedance. Longer antennas were more susceptible to this effect. Short dipoles and monopoles exhibited increases in impedance, but their current distribution was not altered. The loop did not have an altered current distribution; however square loops larger than 3cm a

side were not investigated. Like the small dipole and monopole, the loop did undergo an increase in input impedance at cage resonance. It is possible that the loop must be a certain size to experience the current-altering effects.

Antenna position influenced coupling to the TE_{101}^{z} mode. If the monopole or dipole was moved away from the center of the cage where the $\vec{E}$ field was strongest for the mode, the cavity affected the antenna less. At resonance, if the antenna was moved towards the walls the current distribution shifted back to that of an electrically small antenna, decreasing the input impedance. This effect was seen experimentally by a decreasing S_{21} as the monopole was moved towards the edge of the cage. S_{11} also showed a large decrease in coupling near the walls. The loop coupled magnetically, and had to be located near the walls of the cage where the magnetic fields were dominant. Similar to the dipole and monopole, if the loop was moved away from its region of dominant fields towards the center of the cage, coupling dramatically decreased.

7.2 RF Communication Conclusions

Radio frequency communication is possible inside the wire mesh animal cage. Based on the experimental results of the loop and monopole, coupling to the TE_{101}^{z} mode is best accomplished via the $\vec{E}$ field. The monopole is an electric field dominant antenna, and was shown to couple very well to the cage in Chapter 5. The loop, however, is a magnetic field dominant antenna and as shown in Chapter 6 does not effectively couple to the mode. The worst coupling positions for the monopole still had greater received power than the ideal locations for the loop.

A disadvantage of the monopole is a null that forms around the center of the antenna. This null can be avoided if one monopole is located at the top of the cage and the other is at the

bottom. It was shown in Chapter 5 that the null only extends a certain distance vertically, and if there is enough vertical separation between two monopoles the nulls will never coincide. Ideal placement of the monopole is at the top center of the cage (using the cage wall as a ground plane) where the electric field of TE_{101}^{z} mode is strongest. With one monopole at the top center of the cage, the second can be placed anywhere on the top or bottom and still achieve good coupling.

Larger monopoles were shown to couple better to the cage. The size of the antenna can be reduced but at the sacrifice of received power. Desired power and receiver sensitivity will determine the size of the antennas. Most likely, small transmit antennas will be placed on the animals being monitored. To compensate for this, a larger receiving antenna should be used. There is no advantage to using multiple receive antennas. The top or bottom center of the cage is the best location for receiving a signal, no matter where the transmit antenna is. Additional receive antennas at other positions within the cage will receive less power than the one at the center, even if the transmit antenna is right next to it. Antenna coupling is not dependent on distance, but on the modal distribution of the wire mesh animal cage.

Although the monopole would be difficult to place on an animal, it has demonstrated that $\vec{E}$ field coupling is better than $\vec{H}$ field coupling for the TE_{101}^{z} mode in the wire mesh animal cage. Designs for RF communication system inside the cage should use electric field dominant antennas.

7.3 Future Work

The focus of this thesis was on the possibility of RF communication inside a wire mesh animal cage. Throughout the course of investigating, simulation and experimentation were limited to very simple antennas. All previous work found dealt only with dipole and monopoles.

This thesis included a brief investigation into the loop antenna as well. However, a study into other types of more complex antennas would be advantageous in understanding antenna behavior inside a metallic enclosure. Additionally, varying the size of the antenna produced very interesting results. This was something only briefly touched on by one author [10]. A more in depth investigation into how the size of dipole, monopole, and loop antennas affect coupling and current distribution would be very beneficial. Lastly, a study on antennas that can be placed on small animals would provide a good reference for future work in biotelemetry. This thesis was written without knowledge of what types of antennas would be used. Knowing this would allow for more detailed guidelines to be written on how to implement an RF system to monitor caged animals.

8 Bibliography

[1] P. Sewell, J. D. Turner, M. P. Robinson, and D. W. P. Thomas, “Comparison of analytic, numerical, and approximate models for shielding effectiveness with measurement,” in *IEEE Proc.-Sci. Meas. Technol.*, vol. 145, Mar. 1998, pp. 61–66.

[2] C. M. Butler, Y. Rahmat-Samii, R. Mittra, “Electromagnetic Penetration Through Apertures in Conducting Surfaces,” IEEE Trans. On Electromagnetic Compatibility, Vol. EMC-20, no. 1 Feb, 1978.

[3] H. A. Mendez, *"Shielding theory of enclosures with apertures,”* IEEE Transactions on Electromagnetic Compatibility, Vol. 20, pp. 296-305, May 1978

[4] D.B. Seidel, "*Aperture Excitation of a Wire in a Rectangular Cavity,*" IEEE Transaction on Microwave Theory and Techniques, Vol. 26, pp.908-914, Nov 1978

[5] Robinson, M.P. et al., “*Shielding effectiveness of a rectangular enclosure with a rectangular aperture,”* Electronics Letters, Vo1.32, No.17, August 1996, pp1559-1560.

[6] M. P. Robinson, T. M. Benson, and C. Christopoulos, “Analytical formulation for the shielding effectiveness of enclosures with apertures,” *IEEE Trans. Electromagn. Compat.*, vol. 40, no. 3, pp. 240–248, Aug. 1998.

[7] K. F. Casey, “Electromagnetic Shielding Behavior of Wire-Mesh Screens,” IEEE Transactions on Electromagnetic Compatibility. Vol 30, No 3. pp.298-306, August 1988.

[8] F. Gronwald, “Calculation of Mutual Antenna Coupling Within Rectangular Enclosures,” IEEE Transactions on Electromagnetic Compatibility, Vol. 47, No. 4, Nov. 2005.

[9] Y. Huan, R. Harayanan, “Electromagnetic Coupling Effects on the cavity Measurement of Antenna Efficiency,” IEEE Transactions on Antennas and Propagation, Vol. 51, No. 11, Nov. 2003.

[10] G. Cerri, V. M. Primiani, “Investigation of the Antenna Factor Behavior of a Dipole Operating Inside a Resonant Cavity,” IEEE Transactions on Electromagnetic Compatibility, Vol. 50, No 1. Feb 2008.

[11] F. Gronwald, “Method of Moment Analysis of a Dipole Antenna within a Rectangular Cavity,”

[12] C.A. Balanis, *Advanced Engineering Electromagnetics*, Wiley, 1989, p.602-608

[13] J. A. Black, *UHF Propagation in a Partially Filled Short Cylindrical Waveguide*, Doctoral Dissertation, Marquette University, April 2009.

[14] F.M. Tesche, M. V. Ianoz, T. Karlsson, *EMC Analysis Methods and Computational Models*, Wiley, 1997.

[15] J. Burke, and A. J. Poggio, *Numerical Electromagentics Code (NEC) - Method of Moments Part 1, 2, and 3*," Lawrence Livermore Laboratory, Livermore, CA, Jan. 1981.

[16] J. Burke, E. K. Miller, A. J. Poggio, "*The Numerical Electromagnetics Code (NEC) – A Brief History,"* Lawrence Livermore Laboratory, Livermore, CA, 1990.

[17] See http://home.ict.nl/~arivoors/ for documentation, examples, and 4NEC2 software

[18] J. E. Richie, *The Numerical Electromagnetics Code, NEC*, Tech. Rep. 23, Marquette University ESL, Milwaukee, WI, Jun 20th, 1999.

[19] A. J. Poggio, R. W. Adams, *Approximations for Terms Related to the Kernel in Thin-Wire Integral Equations*, UCRL-51985, Lawrence Livermore Laboratory, CA, December 19, 1975.

[20] C.A. Balanis, *Antenna Theory: Analysis and Design*, Wiley, 1996

[21] W. L. Stutzman, G. A. Theile, *Antenna Theory and Design*, Wiley, Jan. 1997

[22] T. K. Ishii, *Handbook of Microwave Technology: Volume 1*, Academic Press, 1995.

[23] Hines, J.W., Somps, C., Jeutter, D.C. and Singh, A., *Telemetric Sensors for the Space Life Sciences*, IEEE-EMBS Conference, The Netherlands, 1996.

[24] Jeutter DC, *An Academic Perspective on the History and Future of Biotelemetry,* International Telemetry Conference, (Invited), Las Vegas, NV, October 8, 1997.